

## Hierarchical Self-Assembly of Switchable Nucleolipid Supramolecular Gels Based on Environmentally-Sensitive Fluorescent Nucleoside Analogs

Ashok Nuthanakanti and Seergazhi G. Srivatsan\*

Department of Chemistry, Indian Institute of Science Education and Research, Pune  
Dr. Homi Bhabha Road, Pashan, Pune 411008, India

### Electronic Supplementary Information

Content	Page
<b>1. Materials</b>	S2
<b>2. Instrumentation</b>	S2
<b>3. Characterization data for compounds 3a–3d and fluorescent nucleolipids 4-11</b>	S2-S5
<b>4. Fluorescence properties of nucleolipids in different solvents</b>	S5
<b>Fig. S1</b> Strain sweep rheological measurements of nucleolipid gels <b>6 (A)</b> and <b>10 (B)</b>	S5
<b>Fig. S2</b> FESEM image of xerogel of benzothiophene-modified nucleolipid <b>9</b> showing helical ribbon intermediate structures, a possible precursor for nanotubes.	S6
<b>Table S1</b> H-bonding distances and angles, torsional angles and stacking interactions measured from the crystal structures of fluorescent nucleolipids <b>5, 6, 9</b> and <b>10</b> .	S6
<b>Fig. S3</b> Crystal structure showing two molecules of 5-benzofuran-modified nucleolipid <b>5</b> in the asymmetric unit	S7
<b>Fig. S4</b> X-ray crystal structure of nucleolipid <b>5</b> showing strong $\pi$ - $\pi$ stacking interaction	S7
<b>Fig. S5</b> Complete packing diagram of nucleolipid <b>5</b> along the crystallographic a-axes.	S8
<b>Fig. S6</b> X-ray crystal structure of 5-benzofuran-modified nucleolipid <b>6</b> containing palmitoyl acyl chains.	S8
<b>Fig. S7</b> X-ray crystal structure of nucleolipid <b>6</b> showing a detailed view of the H-bonding and stacking interactions.	S9
<b>Fig. S8</b> Complete packing diagram of nucleolipid <b>6</b> along the crystallographic a-axes.	S9
<b>Fig. S9</b> X-ray crystal structures of 5-benzothiophene-modified nucleolipid <b>9 (A)</b> and <b>10 (B)</b> showing one molecule in the unit cell.	S10
<b>Fig. S10</b> Packing diagram of nucleolipid <b>9</b> along the crystallographic a-axes.	S11
<b>Fig. S11</b> X-ray crystal structure showing a detailed view of the H-bonding and stacking interactions in 5-benzothiophene-modified nucleolipid <b>10</b> .	S12
<b>Fig. S12</b> Packing diagram of nucleolipid <b>10</b> along the crystallographic a-axes.	S13
<b>5. Variable temperature <sup>1</sup>H NMR</b>	S13
<b>Fig. S13</b> Partial <sup>1</sup> H NMR spectra of nucleolipid gels of <b>6</b> and <b>10</b> in <i>d</i> <sub>6</sub> -DMSO as a function of increasing temperature.	S14
<b>6. Powder X-ray diffraction (PXRD) analysis of nucleolipids (5, 6, 9 and 10)</b>	S15
<b>Fig. S14</b> PXRD spectra of xerogels of (A) <b>5</b> , (B) <b>6</b> , (C) <b>9</b> , (D) <b>10</b> .	S15
<b>Fig. S15</b> Fluorescence spectra of benzofuran-modified nucleolipid gel <b>5</b> and <b>6</b> at respective CGC as a function of temperature.	S16
<b>Fig. S16</b> Fluorescence spectra of benzothiophene-modified nucleolipid gel <b>9</b> and <b>10</b> at respective CGC as a function of temperature.	S16
<b>Fig. S17</b> Fluorescence spectra of nucleolipid <b>9 (A)</b> and <b>10 (B)</b> at different temperatures.	S17
<b>7. Responsiveness of nucleolipid gel 10 to chemical stimuli.</b>	S17
<b>Fig. S18</b> Partial <sup>1</sup> H NMR spectrum of nucleolipid gel <b>10</b> in <i>d</i> <sub>6</sub> -DMSO (1.4 w/v %) in the absence (A, gel state) and presence of 3 equivalence of fluoride ion (B, sol state).	S18
<b>Fig. S19</b> Plots showing the effect of addition of anions, base and metal ions on the fluorescence intensity ( $\lambda_{em} = 445$ nm) of benzothiophene-modified nucleolipid gel <b>10</b> .	S18
<b>Fig. S20</b> Effect of fluoride ion on UV absorption (A) and fluorescence (B) of nucleolipid <b>10</b>	S19

<b>Fig. S21</b> A plot of emission maximum of benzothiophene-modified uridine nucleoside versus pH.	S19
<b>Fig. S22</b> Partial <sup>1</sup> H NMR spectrum of nucleolipid gel <b>10</b> in <i>d</i> 6-DMSO (1.4 w/v) in the absence (A) and presence of 1 equivalence of Hg <sup>2+</sup> ion (B).	S20
<b>Table S2-S5</b> Crystallographic data for the nucleolipids <b>5, 6, 9 and 10</b>	S20-S22
<b>8. NMR</b>	S23-S30
<b>9. References</b>	S31

**1. Materials:** 5-iodouridine, benzofuran, benzo[*b*]thiophene, butyllithium, tributyltin chloride, bis(triphenylphosphine)palladium(II)dichloride, 4,4'-dimethoxytrityl chloride (DMT-Cl), octanoic acid, oleic acid, palmitic acid, tetrabutylammonium salts, silver nitrate, zinc nitrate hexahydrate, lead(II) nitrate, cadmium acetate dehydrate, mercury(II) perchlorate hexahydrate, DBU (1,8-diazabicyclo(5.4.0) undec-7-ene), dry pyridine were purchased from Sigma-Aldrich. EDC (1-(3-dimethyl aminopropyl)-3-ethyl carbodiimide hydrochloride) and 4-dimethylaminopyridine were obtained from Avra Synthesis. Myristic acid was procured from Fluka. Silicon wafers (N-type without dopant) were purchased from Sigma-Aldrich. 5-Iodo-5'-*O*-DMT-protected uridine **2**,<sup>S1</sup> 2-(tri-*n*-butylstannyl)benzofuran<sup>S2</sup> and 2-(tri-*n*-butylstannyl)benzothiophene<sup>S2</sup> were prepared by following the reported procedures.

**2. Instrumentation:** NMR spectra were recorded on 400 MHz Jeol ECS-400 spectrometer and Bruker 500 MHz spectrometer. Absorption spectra were recorded on a Shimadzu UV-2600 spectrophotometer. Steady-state and time-resolved fluorescence experiments were carried out in a micro fluorescence cuvette (Hellma, path length 1.0 cm) either on a Fluoromax-4 spectrophotometer (Horiba Jobin Yvon) or TCSPC instrument (Horiba Jobin Yvon, Fluorolog-3). The morphology of gels was analyzed using Zeiss Ultra Plus field-emission scanning electron microscope (FESEM). Powder X-ray diffraction (PXRD) spectra were obtained at room temperature using Bruker D8 Advance diffractometer (Cu K $\alpha$  radiation,  $\lambda = 1.5406 \text{ \AA}$ ). Single crystal X-ray data for structure determination were collected from Bruker APEX II DUO diffractometer using MoK $\alpha$  ( $\lambda = 0.71073 \text{ \AA}$ ) graphite monochromated radiation. Gel-sol transition temperature was determined using Equitron round bath clear bottom series medica instrument. MCR-301 (Anton-Paar) rheometer was used for Rheological studies.

### 3. Characterization data for compounds **3a–3d** and fluorescent nucleolipids **4-11**

**Compound 3a:** off white solid, 81% yield. TLC (petroleum ether:EtOAc = 60:40 v/v containing few drops of Et<sub>3</sub>N);  $R_f = 0.48$ ; <sup>1</sup>H NMR (400 MHz, CDCl<sub>3</sub>):  $\delta$  (ppm) 8.11 (s, 1H), 7.46–7.44 (m, 2H), 7.37–7.30 (m, 6H), 7.26–7.22 (m, 1H), 6.87–6.85 (m, 4H), 6.24 (d,  $J = 7.2 \text{ Hz}$ , 1H), 5.67 (dd,  $J_1 = 7.2 \text{ Hz}$ ,  $J_2 = 5.6 \text{ Hz}$ , 1H), 5.59 (dd,  $J_1 = 5.6 \text{ Hz}$ ,  $J_2 = 2.0 \text{ Hz}$ , 1H), 4.21–4.20 (m, 1H), 3.80 (s, 6H), 3.46 (dd,  $J_1 = 10.8 \text{ Hz}$ ,  $J_2 = 2.0 \text{ Hz}$ , 1H), 3.41 (dd,  $J_1 = 11.0 \text{ Hz}$ ,  $J_2 = 2.2 \text{ Hz}$ , 1H), 2.39–2.32 (m, 4H), 1.66–1.59 (m, 4H), 1.33–1.24 (m, 16H), 0.90–0.86 (m, 6H); <sup>13</sup>C NMR (100 MHz, CDCl<sub>3</sub>):  $\delta$  (ppm) 172.8, 172.6, 159.6, 158.9, 150.2, 144.0, 143.9, 135.3, 135.0, 130.3, 130.3, 128.4, 128.3, 127.4, 113.6, 87.8, 85.4, 82.9, 72.8, 71.6, 69.8, 63.1, 55.4, 34.2, 33.9, 31.8, 29.2, 29.2, 29.1, 29.0, 25.0, 24.8, 22.7, 14.2; HRMS: (m/z) calculated for C<sub>46</sub>H<sub>57</sub>IN<sub>2</sub>O<sub>10</sub> [M+Na]<sup>+</sup> = 947.2956, found = 947.2946.

**Compound 3b:** Viscous oil, 77% yield. TLC (petroleum ether:EtOAc = 60:40 v/v containing few drops of Et<sub>3</sub>N);  $R_f = 0.53$ ; <sup>1</sup>H NMR (400 MHz, CDCl<sub>3</sub>):  $\delta$  (ppm) 8.38 (br, 1H), 8.11 (s, 1H), 7.45–7.43 (m, 2H), 7.37–7.30 (m, 6H), 7.25–7.22 (m, 1H), 6.87–6.84 (m, 4H), 6.23 (d,  $J = 7.2 \text{ Hz}$ , 1H), 5.67 (dd,  $J_1 = 7.2 \text{ Hz}$ ,  $J_2 = 5.6 \text{ Hz}$ , 1H), 5.59 (dd,  $J_1 = 5.6 \text{ Hz}$ ,  $J_2 = 2.0 \text{ Hz}$ ,

1H), 4.21–4.20 (m, 1H), 3.79 (s, 6H), 3.45 (dd,  $J_1 = 11.0$  Hz,  $J_2 = 2.2$  Hz, 1H), 3.40 (dd,  $J_1 = 11.0$  Hz,  $J_2 = 2.2$  Hz, 1H), 2.38–2.31 (m, 4H), 1.63 (br, 4H), 1.28–1.25 (m, 40H), 0.89–0.86 (m, 6H);  $^{13}\text{C}$  NMR (100 MHz,  $\text{CDCl}_3$ ):  $\delta$  (ppm) 172.8, 172.7, 158.9, 158.9, 144.0, 136.2, 135.0, 130.3, 130.3, 128.4, 128.3, 127.4, 127.4, 124.9, 113.6, 100.4, 87.8, 85.5, 82.9, 72.8, 71.6, 63.1, 55.4, 34.2, 33.9, 32.1, 29.8, 29.6, 29.5, 29.4, 29.3, 29.3, 25.0, 24.8, 22.8, 14.3; HRMS: (m/z) calculated for  $\text{C}_{58}\text{H}_{81}\text{IN}_2\text{O}_{10}$   $[\text{M}+\text{Na}]^+ = 1115.4834$ , found = 1115.4792.

**Compound 3c:** Viscous oil, 79% yield. TLC (petroleum ether:EtOAc = 60:40 v/v containing few drops of  $\text{Et}_3\text{N}$ );  $R_f = 0.54$ ;  $^1\text{H}$  NMR (400 MHz,  $\text{CDCl}_3$ ):  $\delta$  (ppm) 8.47 (s, 1H), 8.27 (s, 1H), 7.37–7.27 (m, 5H), 7.19–7.17 (m, 2H), 7.16–7.15 (m, 2H), 6.85–6.81 (m, 4H), 6.05 (d,  $J = 6.0$  Hz, 1H), 5.49–5.42 (m, 2H), 4.23–4.20 (m, 1H), 3.99 (dd,  $J_1 = 12.0$  Hz,  $J_2 = 2.0$  Hz, 1H), 3.88 (dd,  $J_1 = 11.4$  Hz,  $J_2 = 1.0$  Hz, 1H), 3.80 (s, 6H), 2.38–2.30 (m, 4H), 1.64–1.59 (m, 4H), 1.28–1.25 (m, 48 H), 0.89–0.86 (m, 6H);  $^{13}\text{C}$  NMR (100 MHz,  $\text{CDCl}_3$ ):  $\delta$  (ppm) 173.0, 172.6, 159.6, 158.7, 150.0, 147.4, 145.3, 144.0, 139.6, 129.3, 128.0, 127.9, 127.2, 113.3, 87.8, 83.9, 73.4, 71.2, 69.2, 62.0, 55.4, 34.1, 33.9, 32.1, 29.9, 29.8, 29.6, 29.5, 29.4, 29.3, 29.2, 25.0, 24.8, 22.8, 14.3; HRMS: (m/z) calculated for  $\text{C}_{62}\text{H}_{89}\text{IN}_2\text{O}_{10}$   $[\text{M}+\text{Na}]^+ = 1171.5460$ , found = 1171.5465.

**Compound 3d:** Viscous oil, 88% yield. TLC (petroleum ether:EtOAc = 60:40 v/v containing few drops of  $\text{Et}_3\text{N}$ );  $R_f = 0.57$ ;  $^1\text{H}$  NMR (400 MHz,  $\text{CDCl}_3$ ):  $\delta$  (ppm) 8.11 (s, 1H), 7.46–7.44 (m, 2H), 7.37–7.30 (m, 6H), 7.25–7.22 (m, 1H), 6.87–6.85 (m, 4H), 6.23 (d,  $J = 7.2$  Hz, 1H), 5.69–5.65 (m, 1H), 5.59 (dd,  $J_1 = 5.4$  Hz,  $J_2 = 2.0$  Hz 1H), 5.38–5.31 (m, 4H), 4.21–4.20 (m, 1H), 3.79 (s, 6H), 3.45 (dd,  $J_1 = 11.0$  Hz,  $J_2 = 2.2$  Hz, 1H), 3.41 (dd,  $J_1 = 10.8$  Hz,  $J_2 = 2.0$  Hz, 1H), 2.39–2.30 (m, 4H), 2.07–1.96 (m, 8H), 1.66–1.60 (m, 4H), 1.30–1.25 (m, 40H), 0.89–0.86 (m, 6H);  $^{13}\text{C}$  NMR (100 MHz,  $\text{CDCl}_3$ ):  $\delta$  (ppm) 172.7, 172.6, 159.7, 158.9, 150.2, 144.0, 135.3, 135.0, 130.3, 130.3, 130.2, 129.8, 129.8, 128.4, 128.3, 128.2, 127.4, 113.6, 87.8, 85.4, 82.9, 72.8, 71.6, 69.7, 63.1, 55.4, 34.1, 33.9, 32.0, 29.9, 29.9, 29.7, 29.5, 29.3, 29.3, 27.4, 27.3, 25.0, 24.8, 22.8, 14.3; HRMS: (m/z) calculated for  $\text{C}_{66}\text{H}_{93}\text{IN}_2\text{O}_{10}$   $[\text{M}+\text{Na}]^+ = 1223.5773$ , found = 1223.5764.

**Compound 4:** Off white solid, 77% yield over two steps. TLC (petroleum ether:EtOAc = 70:30);  $R_f = 0.54$ ;  $^1\text{H}$  NMR (400 MHz,  $\text{CDCl}_3$ ):  $\delta$  (ppm) 9.13 (s, 1H), 8.40 (s, 1H), 7.56–7.53 (m, 1H), 7.46–7.45 (m, 1H), 7.40–7.38 (m, 1H), 7.27–7.17 (m, 2H), 6.09 (d,  $J = 6.4$  Hz, 1H), 5.66 (t,  $J = 6.0$  Hz, 1H), 5.57 (dd,  $J_1 = 6.0$  Hz,  $J_2 = 3.2$  Hz, 1H), 4.26 (dd,  $J_1 = 5.2$  Hz,  $J_2 = 2.4$  Hz, 1H), 4.05 (dd,  $J_1 = 12.0$  Hz,  $J_2 = 2.4$  Hz, 1H), 3.94 (dd,  $J_1 = 12.4$  Hz,  $J_2 = 2.4$  Hz, 1H), 2.41–2.31 (m, 4H), 1.69–1.55 (m, 4H), 1.36–1.20 (m, 16 Hz), 0.91–0.83 (m, 6H);  $^{13}\text{C}$  NMR (100 MHz,  $\text{CDCl}_3$ ):  $\delta$  (ppm) 173.0, 172.7, 160.0, 153.8, 149.5, 147.5, 136.7, 129.2, 124.8, 123.2, 121.6, 110.7, 107.4, 106.4, 89.4, 84.1, 73.0, 71.2, 62.2, 34.2, 33.9, 31.8, 31.7, 29.2, 29.2, 29.1, 29.0, 25.0, 24.8, 22.7, 22.7, 14.2; HRMS: (m/z) calculated for  $\text{C}_{33}\text{H}_{44}\text{N}_2\text{O}_9$   $[\text{M}+\text{Na}]^+ = 635.2945$ , found = 635.2934.

**Compound 5:** Off white solid, 66% yield over two steps. TLC (petroleum ether:EtOAc = 70:30);  $R_f = 0.42$ ;  $^1\text{H}$  NMR (400 MHz,  $\text{CDCl}_3$ ):  $\delta$  (ppm) 8.80 (br, 1H), 8.40 (s, 1H), 7.57–7.54 (m, 1H), 7.49–7.47 (m, 1H), 7.41–7.39 (m, 1H), 7.32–7.28 (m, 1H), 7.24–7.19 (m, 1H), 6.09 (d,  $J = 6.4$  Hz, 1H), 5.65 (t,  $J = 6.0$  Hz, 1H), 5.57 (dd,  $J_1 = 5.6$  Hz,  $J_2 = 3.2$  Hz, 1H), 4.26 (dd,  $J_1 = 5.2$  Hz,  $J_2 = 2.0$  Hz, 1H), 4.05 (dd,  $J_1 = 12.2$  Hz,  $J_2 = 2.2$  Hz, 1H), 3.94 (dd,  $J_1 = 12.4$  Hz,  $J_2 = 2.2$  Hz, 1H), 2.40–2.31 (m, 4H), 1.68–1.57 (m, 4H), 1.32–1.23 (m, 40), 0.90–0.85 (m, 6H);  $^{13}\text{C}$  NMR (100 MHz,  $\text{CDCl}_3$ ):  $\delta$  (ppm) 172.9, 172.6, 159.7, 153.8, 149.4, 147.5, 136.6, 129.2, 124.8, 123.2, 121.6, 110.7, 107.4, 106.4, 89.4, 84.1, 73.0, 71.2,

62.2, 34.2, 33.9, 32.1, 29.8, 29.6, 29.5, 29.5, 29.4, 29.3, 29.2, 28.0, 27.0, 25.0, 24.9, 22.8, 14.3; HRMS: (m/z) calculated for C<sub>45</sub>H<sub>68</sub>N<sub>2</sub>O<sub>8</sub> [M+Na]<sup>+</sup> = 803.4822, found = 803.4835.

**Compound 6:** Off white solid, 69% yield over two steps. TLC (petroleum ether:EtOAc = 70:30); *R<sub>f</sub>* = 0.56; <sup>1</sup>H NMR (400 MHz, CDCl<sub>3</sub>): δ (ppm) 8.40 (br, 1H), 7.57–7.55 (m, 1H), 7.47 (br, 1H), 7.41–7.39 (m, 1H), 7.28–7.26 (m, 1H), 7.24–7.19 (m, 1H), 6.09 (d, *J* = 6.4 Hz, 1H), 5.65 (t, *J* = 6.0 Hz, 1H), 5.57 (dd, *J*<sub>1</sub> = 5.6 Hz, *J*<sub>2</sub> = 3.2 Hz, 1H), 4.26 (dd, *J*<sub>1</sub> = 5.2 Hz, *J*<sub>2</sub> = 2.4 Hz, 1H), 4.05 (dd, *J*<sub>1</sub> = 12.0 Hz, *J*<sub>2</sub> = 2.4 Hz, 1H), 3.94 (dd, *J*<sub>1</sub> = 12.0 Hz, *J*<sub>2</sub> = 2.4 Hz, 1H), 2.38–2.31 (m, 4H), 1.68–1.55 (m, 4H), 1.29–1.22 (m, 48H), 0.90–0.85 (m, 6H); <sup>13</sup>C NMR (100 MHz, CDCl<sub>3</sub>): δ (ppm) 173.4, 173.4, 160.3, 153.7, 150.2, 147.4, 134.5, 129.1, 124.9, 123.3, 121.5, 110.6, 107.3, 106.4, 89.7, 80.9, 74.1, 72.1, 63.3, 34.1, 34.0, 32.1, 29.8, 29.8, 29.7, 29.6, 29.5, 29.5, 29.4, 29.4, 29.3, 29.2, 24.9, 22.8, 14.3; HRMS: (m/z) calculated for C<sub>49</sub>H<sub>76</sub>N<sub>2</sub>O<sub>9</sub> [M+Na]<sup>+</sup> = 859.5449, found = 859.5482.

**Compound 7:** Viscous oil, 39% yield over two steps. TLC (petroleum ether:EtOAc = 70:30); *R<sub>f</sub>* = 0.49; <sup>1</sup>H NMR (400 MHz, CDCl<sub>3</sub>): δ (ppm) 8.99 (s, 1H), 8.41 (s, 1H), 7.57–7.56 (m, 1H), 7.46 (br, 1H), 7.41–7.39 (m, 1H), 7.28–7.26 (m, 1H), 7.24–7.18 (m, 1H), 6.09 (d, *J* = 6.0 Hz, 1H), 5.65 (t, *J* = 6.0 Hz, 1H), 5.57 (dd, *J*<sub>1</sub> = 5.6 Hz, *J*<sub>2</sub> = 3.2 Hz, 1H), 5.39–5.28 (m, 4H), 4.29–4.24 (m, 1H), 4.05 (dd, *J*<sub>1</sub> = 12.2 Hz, *J*<sub>2</sub> = 2.2 Hz, 1H), 3.94 (dd, *J*<sub>1</sub> = 12.0 Hz, *J*<sub>2</sub> = 2.0 Hz, 1H), 2.40–2.31 (m, 4H), 2.07–1.91 (m, 8H), 1.66–1.55 (m, 4H), 1.32–1.22 (m, 40H), 0.89–0.85 (m, 6H); <sup>13</sup>C NMR (100 MHz, CDCl<sub>3</sub>): δ (ppm) 172.9, 172.6, 159.9, 153.8, 149.4, 147.5, 136.6, 130.2, 130.2, 129.8, 129.2, 124.8, 123.2, 121.6, 110.7, 107.4, 106.4, 89.3, 84.1, 73.0, 71.2, 62.2, 34.1, 33.9, 32.0, 29.9, 29.8, 29.8, 29.7, 29.5, 29.4, 29.3, 29.2, 27.4, 27.3, 25.0, 24.8, 22.8, 14.3; HRMS: (m/z) calculated for C<sub>53</sub>H<sub>80</sub>N<sub>2</sub>O<sub>9</sub> [M+Na]<sup>+</sup> = 911.5762, found = 911.5715.

**Compound 8:** Off white solid, 67% yield over two steps. TLC (EtOAc:hexane = 30:70); *R<sub>f</sub>* = 0.29; <sup>1</sup>H NMR (400 MHz, CDCl<sub>3</sub>): δ (ppm) 8.81 (s, 1H), 8.36 (s, 1H), 7.89 (s, 1H), 7.76–7.71 (m, 2H), 7.34–7.27 (m, 2H), 6.20 (d, *J* = 5.2 Hz, 1H), 5.59–5.52 (m, 2H), 4.28–4.27 (m, 1H), 4.07 (dd, *J*<sub>1</sub> = 12.0 Hz, *J*<sub>2</sub> = 1.6 Hz, 1H), 3.96 (dd, *J*<sub>1</sub> = 11.6 Hz, *J*<sub>2</sub> = 1.2 Hz, 1H), 2.41–2.32 (m, 4H), 1.68–1.56 (m, 4H), 1.37–1.21 (m, 16H), 0.91–0.84 (m, 6H); <sup>13</sup>C NMR (100 MHz, CDCl<sub>3</sub>): δ (ppm) 173.1, 172.7, 160.7, 149.4, 140.1, 138.7, 136.9, 133.8, 124.8, 124.8, 123.9, 122.8, 121.9, 110.7, 87.9, 84.0, 73.6, 71.4, 62.2, 34.2, 33.9, 31.8, 31.8, 29.2, 29.2, 29.1, 29.0, 25.0, 24.8, 22.7, 22.7, 14.2; HRMS: (m/z) calculated for C<sub>33</sub>H<sub>44</sub>N<sub>2</sub>O<sub>8</sub>S [M+Na]<sup>+</sup> = 651.2715, found = 651.2712.

**Compound 9:** Off white solid, 70% yield over two steps. TLC (EtOAc:hexane = 30:70); *R<sub>f</sub>* = 0.41; <sup>1</sup>H NMR (400 MHz, CDCl<sub>3</sub>): δ (ppm) 8.68–8.62 (br, 1H), 8.37 (s, 1H), 7.89 (s, 1H), 7.77–7.72 (m, 2H), 7.34–7.27 (m, 2H), 6.2 (d, *J* = 5.6 Hz, 1H), 5.57–5.53 (m, 2H), 4.27–4.26 (m, 1H), 4.08–4.05 (m, 1H), 3.97–3.94 (m, 1H), 2.40–2.32 (m, 4H), 1.67–1.64 (m, 4H), 1.31–1.24 (m, 40H), 0.89–0.85 (m, 6H); <sup>13</sup>C NMR (100 MHz, CDCl<sub>3</sub>): δ (ppm) 173.1, 172.7, 160.6, 149.4, 140.1, 138.7, 136.9, 133.9, 124.8, 124.6, 123.9, 122.8, 121.9, 110.7, 87.8, 84.0, 73.6, 71.4, 62.2, 34.2, 34.0, 32.1, 29.8, 29.8, 29.6, 29.5, 29.4, 29.3, 29.2, 25.0, 24.9, 22.8, 14.3; HRMS: (m/z) calculated for C<sub>45</sub>H<sub>68</sub>N<sub>2</sub>O<sub>8</sub>S [M+Na]<sup>+</sup> = 819.4594, found = 819.4597.

**Compound 10:** Off white solid, 77% yield over two steps. TLC (EtOAc:hexane = 40:60); *R<sub>f</sub>* = 0.72; <sup>1</sup>H NMR (400 MHz, CDCl<sub>3</sub>): δ (ppm) 8.37 (s, 1H), 7.90–7.89 (s, 1H), 7.76–7.72 (m, 2H), 7.34–7.29 (m, 2H), 6.20 (d, *J* = 4.8 Hz, 1H), 5.58–5.55 (m, 2H), 4.27 (br, 1H), 4.08–4.05 (m, 1H), 3.97–3.94 (m, 1H), 2.40–2.32 (m, 4H), 1.68–1.56 (m, 4H), 1.36–1.23 (m, 48H),

0.89–0.86 (m, 6H);  $^{13}\text{C}$  NMR (100 MHz,  $\text{CDCl}_3$ ):  $\delta$  (ppm) 173.1, 172.7, 160.6, 149.4, 140.1, 138.7, 136.9, 133.8, 124.8, 124.6, 123.9, 122.8, 121.9, 121.1, 110.7, 87.9, 84.0, 73.6, 71.4, 62.2, 34.2, 34.0, 32.1, 29.9, 29.8, 29.6, 29.5, 29.4, 29.4, 29.3, 29.2, 25.0, 24.9, 22.8, 14.3; HRMS: (m/z) calculated for  $\text{C}_{49}\text{H}_{76}\text{N}_2\text{O}_8\text{S}$   $[\text{M}+\text{Na}]^+ = 875.5220$ , found = 875.5190.

**Compound 11:** Viscous oil, 47% yield over two steps. TLC (EtOAc:hexane = 30:70);  $R_f = 0.40$ ;  $^1\text{H}$  NMR (400 MHz,  $\text{CDCl}_3$ ):  $\delta$  (ppm) 8.68 (s, 1H), 8.37 (s, 1H), 7.89 (s, 1H), 7.76–7.72 (m, 2H), 7.34–7.27 (m, 2H), 6.20 (d,  $J = 5.2$  Hz, 1H), 5.58–5.53 (m, 2H), 5.38–5.28 (m, 4H), 4.27–4.26 (m, 1H), 4.07 (dd,  $J_1 = 12.0$  Hz,  $J_2 = 2.0$  Hz, 1H), 3.96 (dd,  $J_1 = 11.8$  Hz,  $J_2 = 1.8$  Hz, 1H), 2.40–2.32 (m, 4H), 2.07–1.91 (m, 8H), 1.68–1.56 (m, 4H), 1.32–1.23 (m, 40H), 0.89–0.86 (m, 6H);  $^{13}\text{C}$  NMR (100 MHz,  $\text{CDCl}_3$ ):  $\delta$  (ppm) 173.0, 172.7, 160.6, 149.4, 140.1, 138.7, 136.9, 133.9, 130.2, 130.2, 129.8, 129.8, 124.8, 124.6, 123.9, 122.8, 121.9, 110.7, 87.8, 84.0, 73.6, 71.4, 62.2, 34.1, 33.9, 32.0, 29.9, 29.8, 29.7, 29.5, 29.4, 29.3, 29.2, 27.4, 27.3, 25.0, 24.8, 22.8, 14.3; HRMS: (m/z) calculated for  $\text{C}_{53}\text{H}_{80}\text{N}_2\text{O}_8\text{S}$   $[\text{M}+\text{Na}]^+ = 927.5533$ , found = 927.5550.

#### 4. Fluorescence properties of nucleolipids in different solvents:

*Quantum yield of nucleolipids in various solvents:* Quantum yield of 5-benzofuran-modified (**5** and **6**) and 5-benzothiophene-modified (**9** and **10**) nucleolipids in different solvents relative to 2-aminopurine as the standard was determined using the following equation.<sup>S3</sup>

$$\Phi_{\text{F}(x)} = \left(\frac{A_s}{A_x}\right) \left(\frac{F_x}{F_s}\right) \left(\frac{n_x}{n_s}\right)^2 \Phi_{\text{F}(s)}$$

Where s is the standard, x is the nucleolipid, A is the absorbance at excitation wavelength, F is the area under the emission curve, n is the refractive index of the solvent, and  $\Phi_{\text{F}}$  is the quantum yield. Quantum yield of 2-aminopurine in water is 0.68.<sup>S4</sup>

*Steady-state fluorescence anisotropy measurements:* Steady-state fluorescence anisotropy measurements in different solvents were performed by exciting the samples (5  $\mu\text{M}$ ) at 320 nm. The anisotropy value ( $r$ ) was determined by analyzing the data using software provided with the instrument. Anisotropy measurements were performed in duplicate and the values reported in this study are an average of ten successive measurements for each sample.

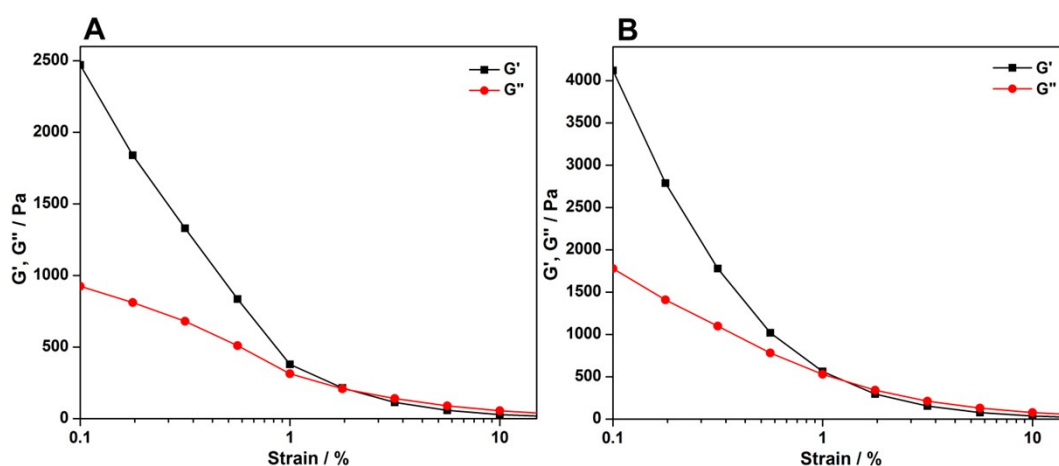


**Fig. S1** Strain sweep rheological measurements of nucleolipid gels **6** (A) and **10** (B) at respective CGC in DMSO at constant oscillating frequency.

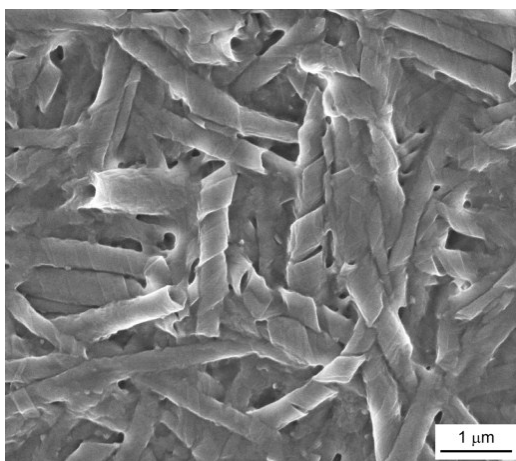


**Fig. S2** FESEM image of xerogel of benzothiophene-modified nucleolipid **9** showing helical ribbon intermediate structures, a possible precursor for nanotubes.

**Table S1** H-bonding distances and angles, torsional angles and  $\pi$ - $\pi$  interactions measured from the crystal structure of fluorescent nucleolipids **5**, **6**, **9** and **10**.

nucleolipid	hydrogen bond	distance (Å)	angle (°)	torsion angle ( $\chi$ ) (°)	$\pi$ - $\pi$ distance (Å)
<b>5</b>	N3AH---O4B	2.011(5)	167.6(4)	C2A-N1A-C1'A-O4'A 149.7(4)	C11A----C12B 3.594(1)
	O2A---HN3B	1.990(5)	166.5(4)	C2B-N1B-C1'B-O4'B 130.0(4)	C12A----C13B 3.448(9)
	O5'AH---O5'B	1.990(7)	154.2(5)		
	C6BH---O5'B	2.288(5)	157.6(4)		
<b>6</b>	N3AH---O4B	2.003(12)	166.9(1)	C2A-N1A-C1'A-O4'A 151.2(1)	C11A----C12B 3.583(2)
	O2A---HN3B	2.003(12)	168.3(1)	C2B-N1B-C1'B-O4'B 129.9(1)	C12A----C13B 3.468(2)
	O5'AH---O5'B	1.945(16)	167.3(2)		
	C6BH---O5'B	2.296(13)	155.9(1)		
<b>9</b>	N3H---O29	2.034(1)	170.6(1)	C2-N1-C1'-O4' 236.8(1)	C4----S1 3.387(2)
	O4'---HO5'	2.021(2)	162.3(1)		C8----C13 3.390(2)
	C6H---O5'	2.403(2)	157.6(1)		
<b>10</b>	N3H---O6	2.033(2)	168.5(1)	C2-N1-C1'-O4' 237.2(2)	C4----S1 3.324(3)
	O4'---O5' <sup>[a]</sup>	2.792(3)	-		C8----C13 3.358(3)
	C6H---O5'	2.374(3)	159.4(1)		

<sup>[a]</sup>The position of hydrogen atom of 5'-OH could not be fixed satisfactorily and hence, O4'---O5' distance is given.

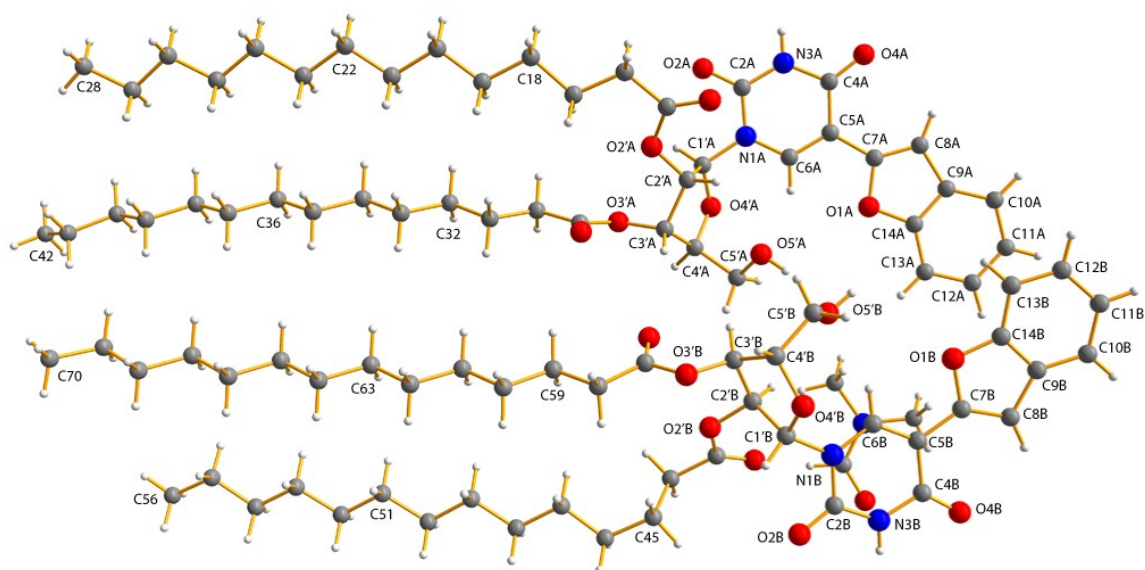


**Fig. S3** Crystal structure showing two molecules of 5-benzofuran-modified nucleolipid **5** in the asymmetric unit, which are designated as A and B. Solvent (DMF) has not been labeled for clarity. The uracil and benzofuran rings are almost coplanar. Modified nucleobase adopts an *anti* conformation relative to the sugar ring with C3'-*exo* sugar puckering. Atoms are coded as follows: off white, hydrogen; dark gray, carbon; blue, nitrogen; red, oxygen.

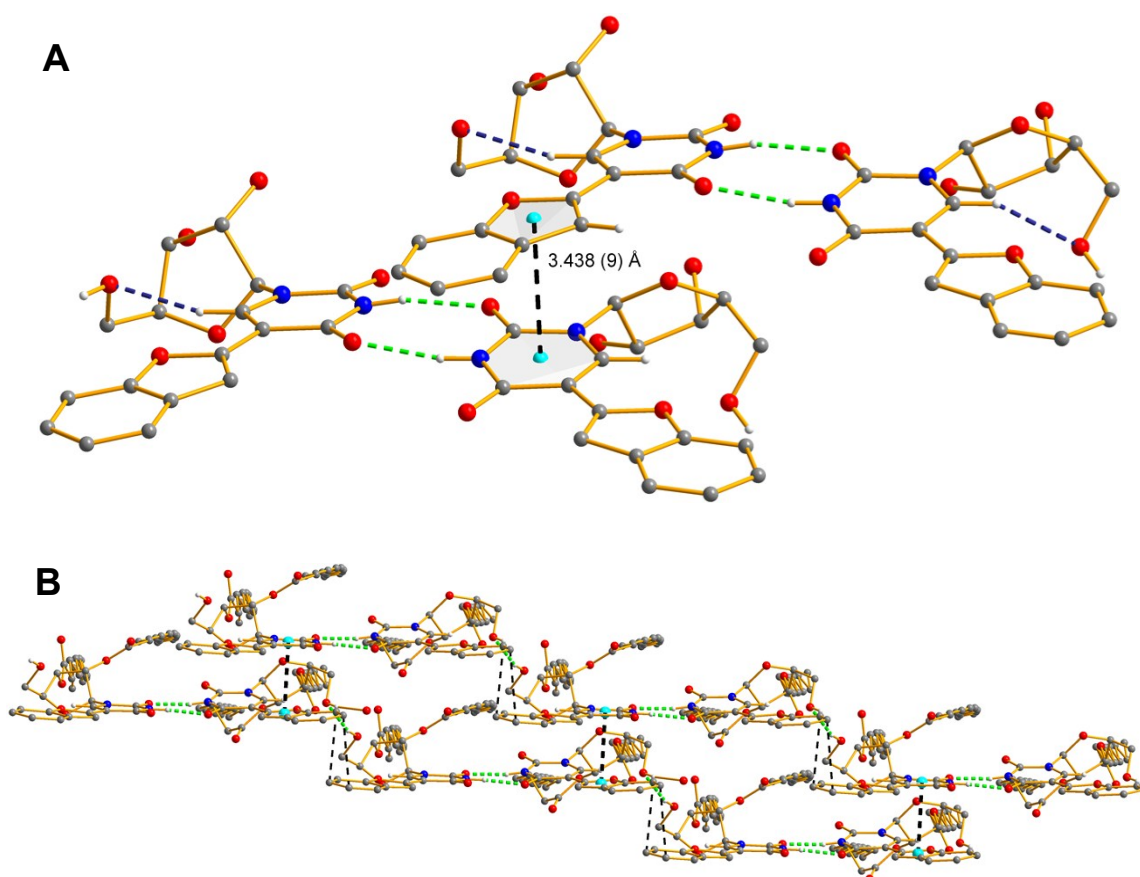


**Fig. S4** (A) X-ray crystal structure of nucleolipid **5** showing strong  $\pi$ - $\pi$  stacking interaction between the uracil ring of one layer and furan ring of benzofuran moiety of the next layer.  $\pi$ - $\pi$  stacking distance (3.438 Å) between the uracil and furan rings is shown in black dashed lines. (B) Layered supramolecular architecture formed by various non-covalent interactions. Hydrogen atoms are omitted for clarity and atom labels are same as in Figure S3†.

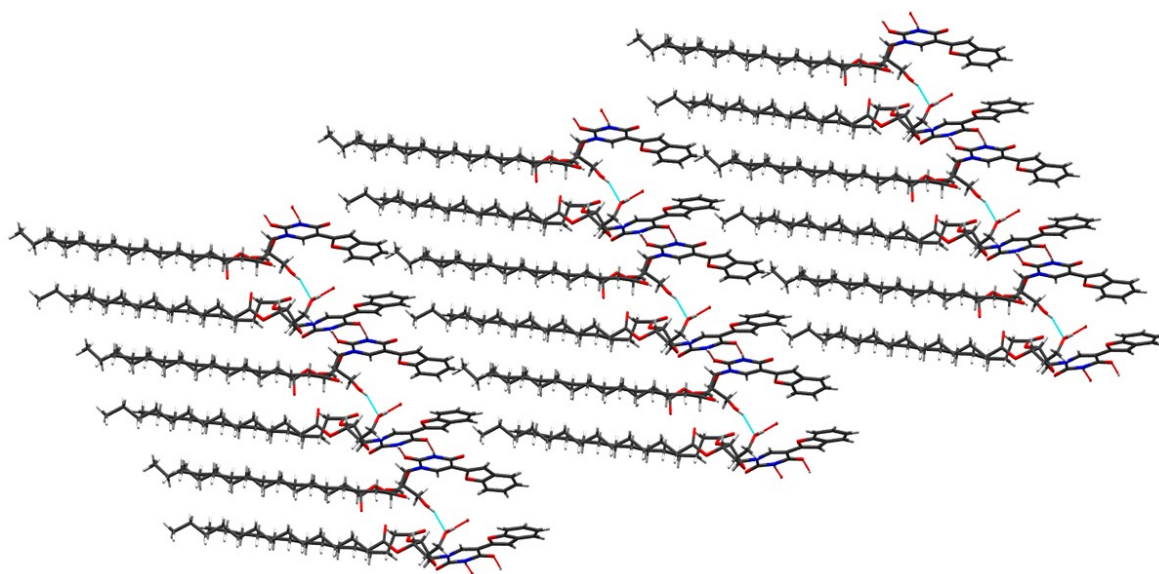


**Fig. S5** Packing diagram of nucleolipid **5** along the crystallographic a-axis.

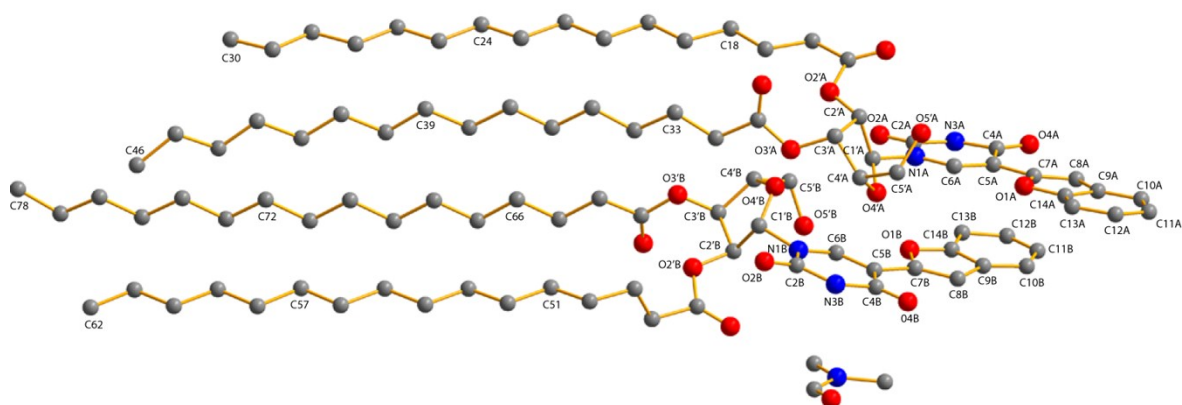


**Fig. S6** X-ray crystal structure of 5-benzofuran-modified nucleolipid **6** containing palmitoyl acyl chains. Crystal structure shows two molecules of **6** in the asymmetric unit, which are designated as A and B. Solvent (DMF) has not been labeled for clarity. Akin to **5**, the uracil and benzofuran rings in **6** are almost coplanar. Modified nucleobase adopts an *anti* conformation relative to the sugar ring with C3'-*exo* sugar puckering. Hydrogen atoms were omitted for clarity. Atoms are coded as follows: dark gray, carbon; blue, nitrogen; red, oxygen.

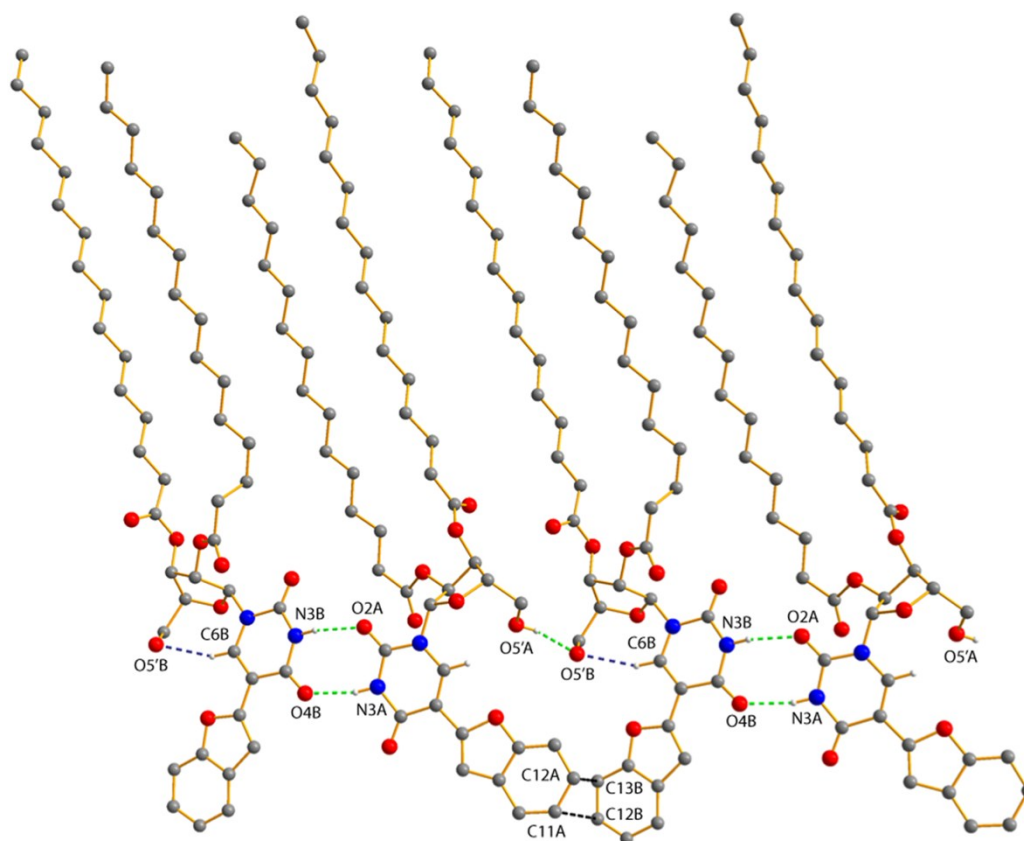


**Fig. S7** X-ray crystal structure of nucleolipid **6** showing a detailed view of the H-bonding and  $\pi$ - $\pi$  interactions. Canonical intermolecular H-bonding interactions (base pair and O5'AH---O5'B) are shown in green dashed lines. Intramolecular H-bond C6BH---O5'B is shown in dark blue dashed lines. Atoms involved in partial  $\pi$ - $\pi$  stacking interaction (C11A-C12B and C12A-C13B) are shown in black dashed lines. Hydrogen atoms not involved in H-bonding are omitted for clarity. Atoms are coded as follows: off white, hydrogen; dark gray, carbon; blue, nitrogen; red, oxygen.

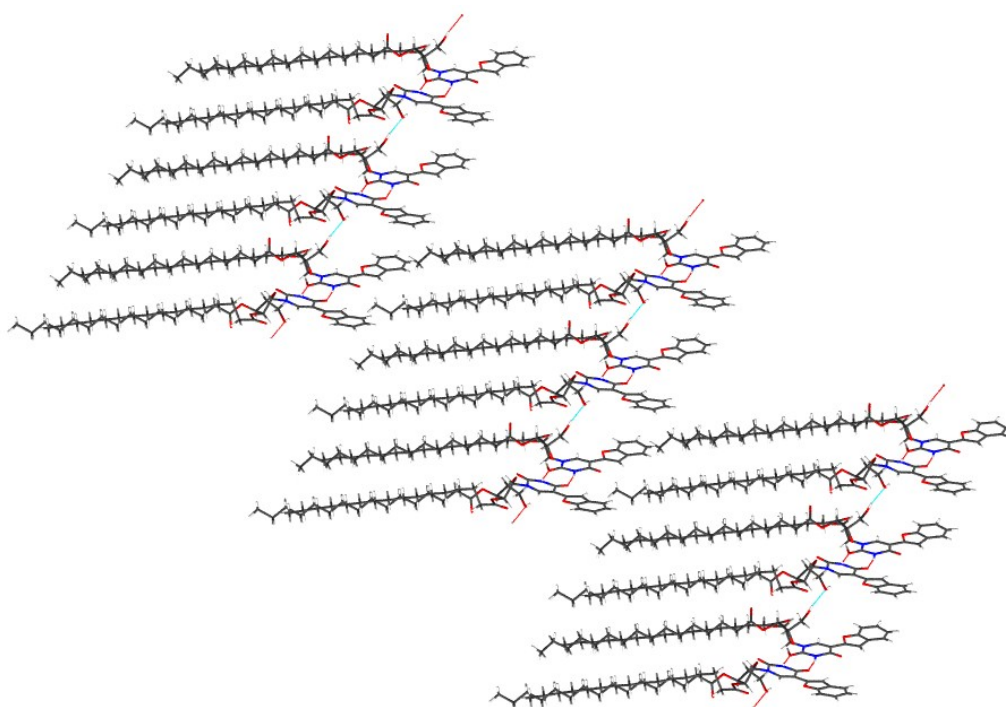


**Fig. S8** Packing diagram of nucleolipid **6** along the crystallographic a-axis.

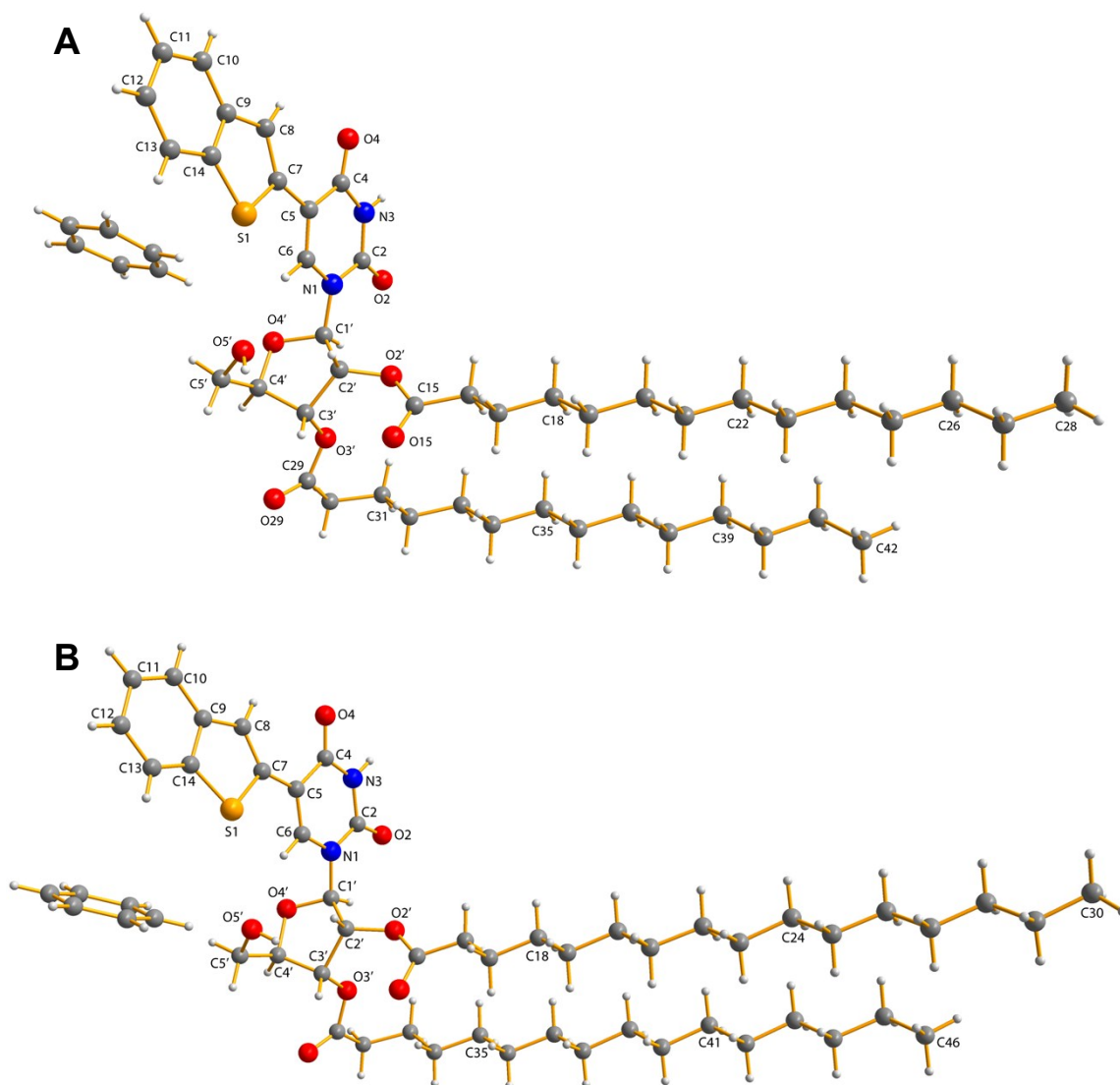


**Fig. S9** X-ray crystal structures of 5-benzothiophene-modified nucleolipid **9** (A) and **10** (B) showing one molecule in the unit cell. Uracil and benzothiophene rings are not coplanar. Modified nucleobase adopts an *anti* conformation relative to the sugar ring with C3'-*exo* sugar pucker. Atoms are coded as follows: off white, hydrogen, dark gray, carbon; blue, nitrogen; red, oxygen; golden yellow, sulfur.

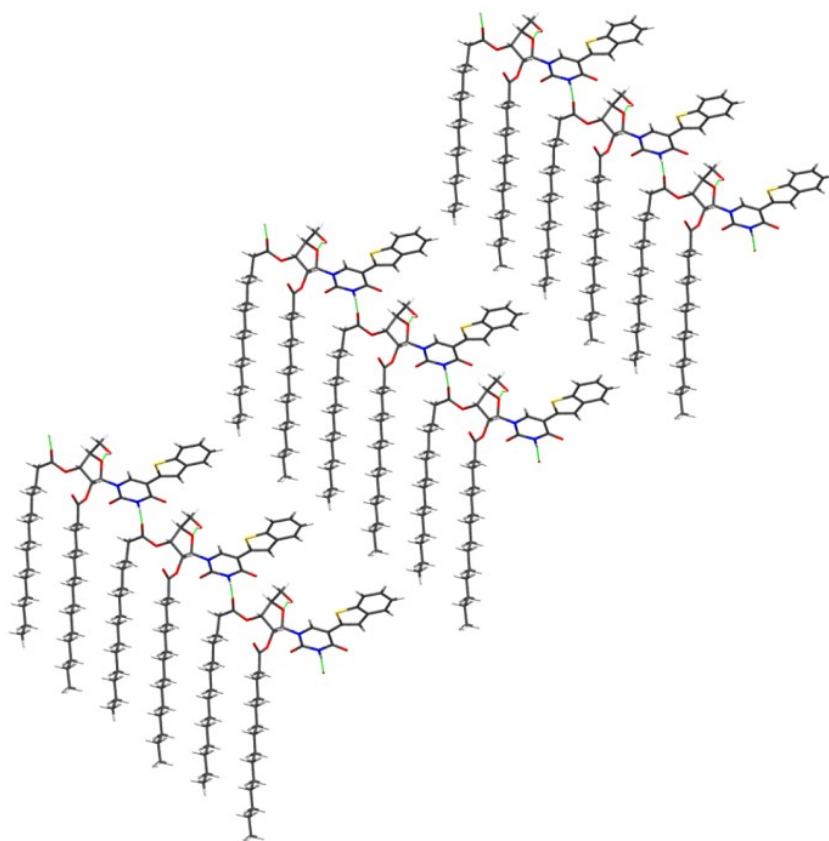


**Fig. S10** Packing diagram of nucleolipid **9** along the crystallographic a-axes.

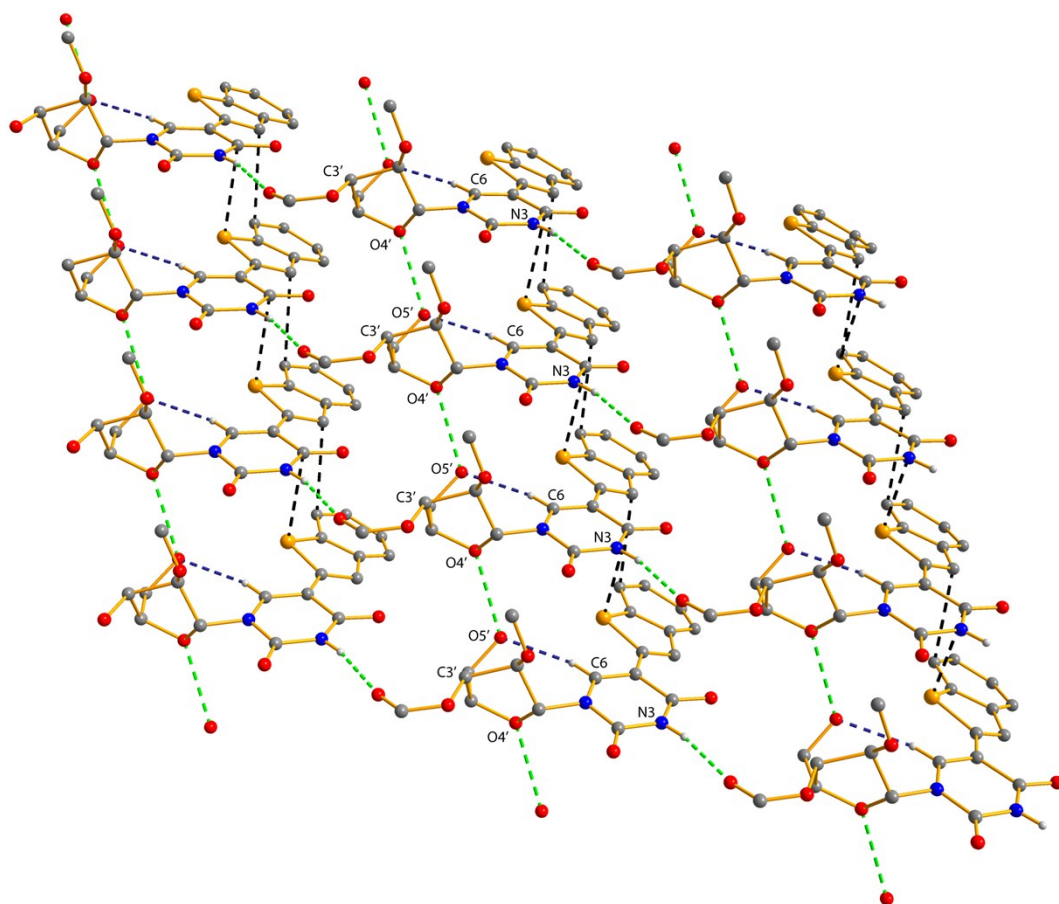


**Fig. S11** X-ray crystal structure showing a detailed view of the H-bonding and  $\pi$ - $\pi$  interactions in 5-benzothiophene-modified nucleolipid **10**. Intermolecular H-bonding interactions are shown in green dashed lines. Intramolecular H-bond C6H---O5' is shown in dark blue dashed lines. Atoms involved in partial  $\pi$ - $\pi$  stacking interaction are shown in black dashed lines. See Table S1 for details. Hydrogen atoms not involved in H-bonding and part of the fatty acid acyl chains have been omitted for clarity. Atoms are coded as follows: off white, hydrogen; dark gray, carbon; blue, nitrogen; red, oxygen; golden yellow, sulfur.

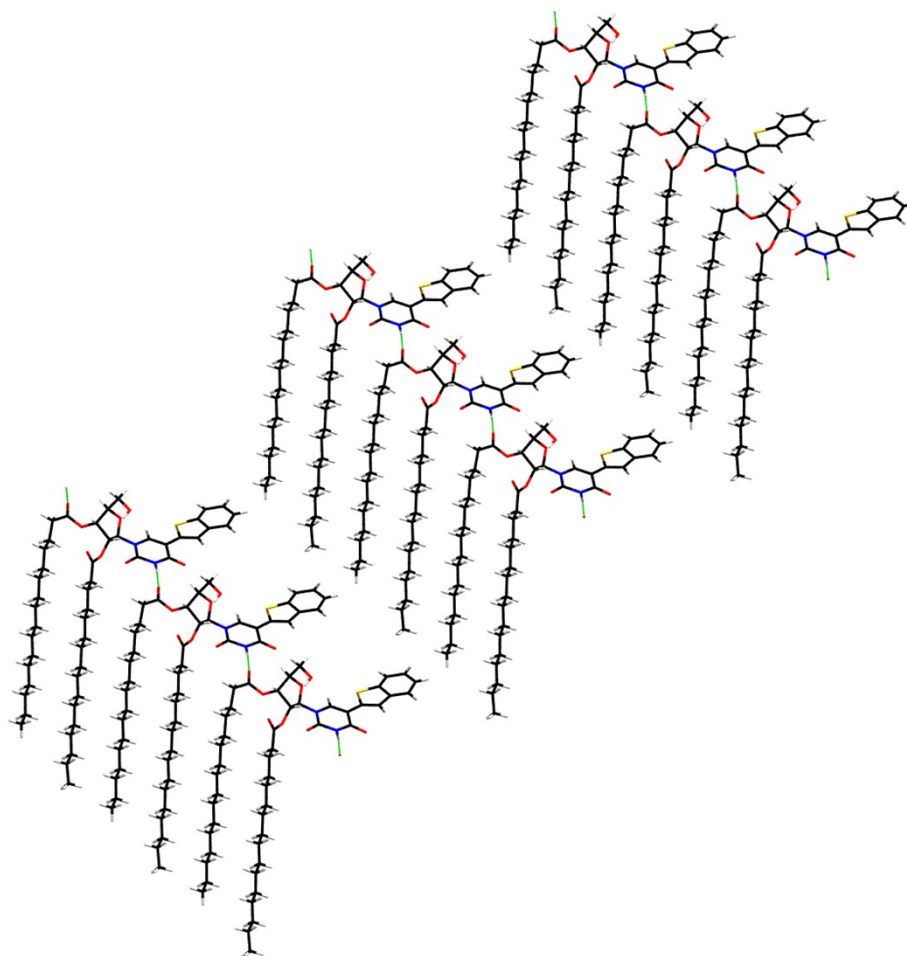


**Fig. S12** Packing diagram of nucleolipid **10** along the crystallographic a-axes.

**5. Variable temperature  $^1\text{H}$  NMR:** Gels of **6** (0.9 w/v %) and **10** (1.4 w/v %) in *d6*-DMSO were formed in individual NMR tubes by heating and cooling process.  $^1\text{H}$  NMR was recorded on a 500 MHz spectrometer as a function of increasing temperature. The temperature of the sample was increased from 25 °C to 55 °C with an increment of 5 °C and equilibration time of 10 min. The spectrum was recorded at every 5 °C interval.

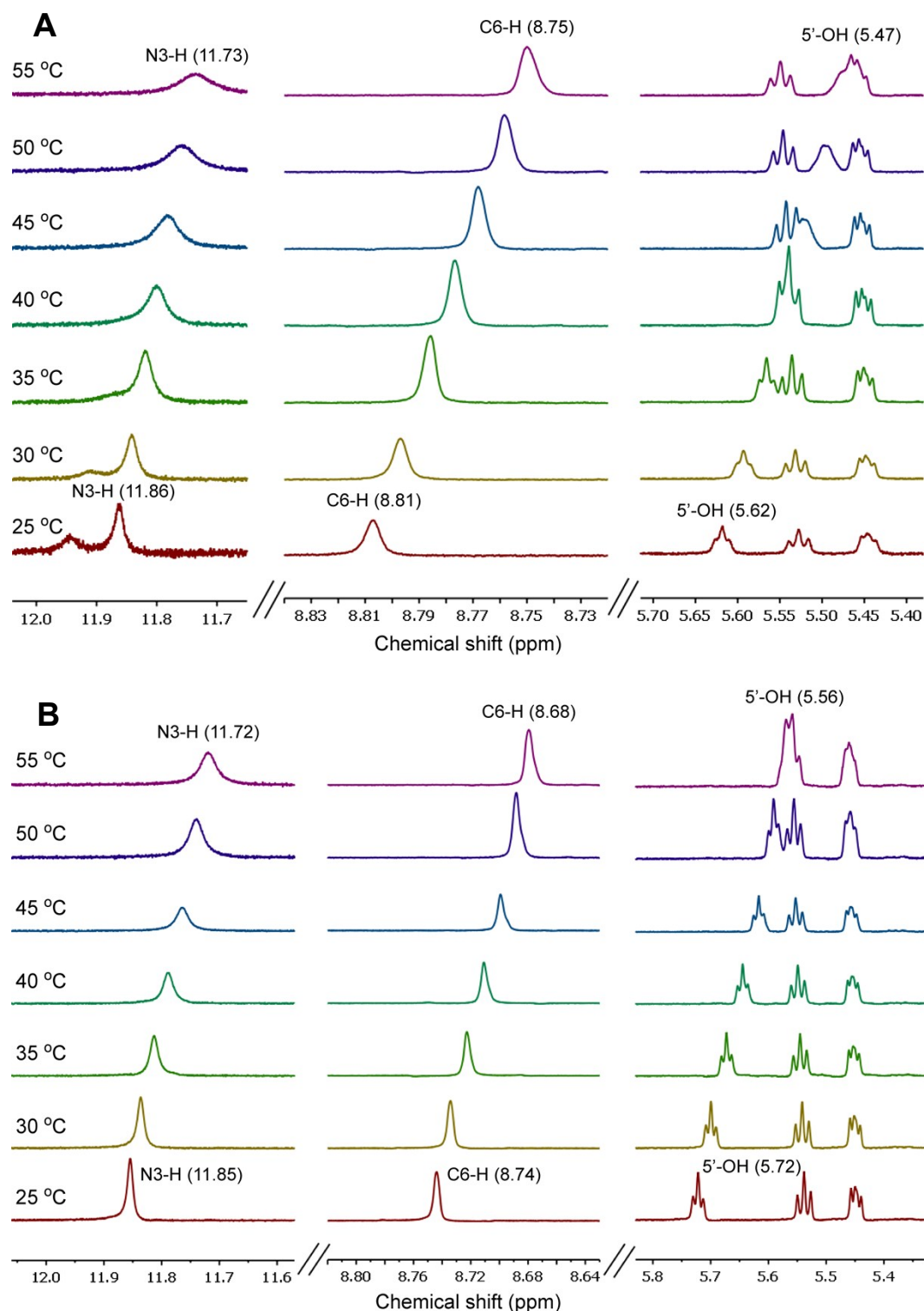


**Fig. S13** Partial  $^1\text{H}$  NMR spectra of nucleolipid gels of **6** (A) and **10** (B) in  $d_6$ -DMSO as a function of increasing temperature. N3-H and 5'-OH, which participated in strong intermolecular H-bonding in crystalline state, exhibited significant upfield shift in their proton signals during gel-sol transition. C6H of nucleobase, which participated in a weak intramolecular C-H-O H-bonding interaction, also showed small upfield shift during gel-sol transition. These results indicate that the H-bonding interactions in crystal structure and in supramolecular gel are similar. For experimental details see section 5.

**6. Powder X-ray diffraction (PXRD) analysis of nucleolipids 5, 6, 9 and 10:** A hot solution of nucleolipid in DMSO at respective CGC was drop-casted on glass slide and was allowed to form gel at RT. The glass slide was placed in a vacuum desiccator and was dried under vacuum for nearly 15 h to obtain the xerogel. PXRD data was collected using Bruker D8 Advance diffractometer with CuK $\alpha$  source (1.5406 Å). Diffraction data were collected at 2 $\theta$  angle from 1° to 40° using a 0.01° step size and 0.5 s per step. Low angle diffraction data was collected by keeping the motorized divergence slit in automatic mode so as to maintain the X-ray beam footprint on the sample to 12 x 12 mm. Further, the position sensitive detector (Lynxeye) channels were reduced to minimize the background X-ray scattering entering the detector.

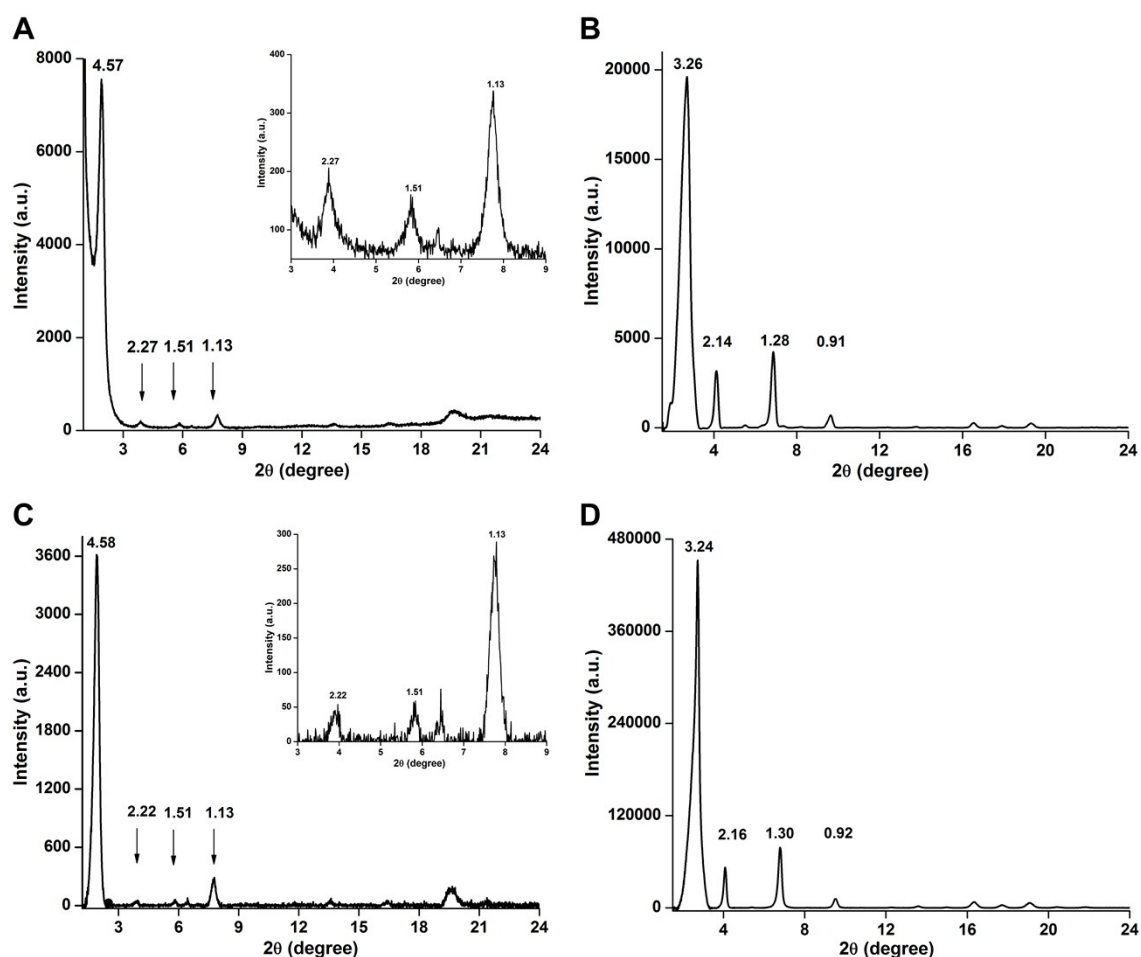


**Fig. S14** PXRD spectra of xerogels of (A) 5, (B) 6, (C) 9, (D) 10. Inset in (A) and (C): peaks in the 2 $\theta$  value range of 3–9° have been magnified. Layer spacing (nm) for prominent diffraction peaks are also given. For details see section 6.

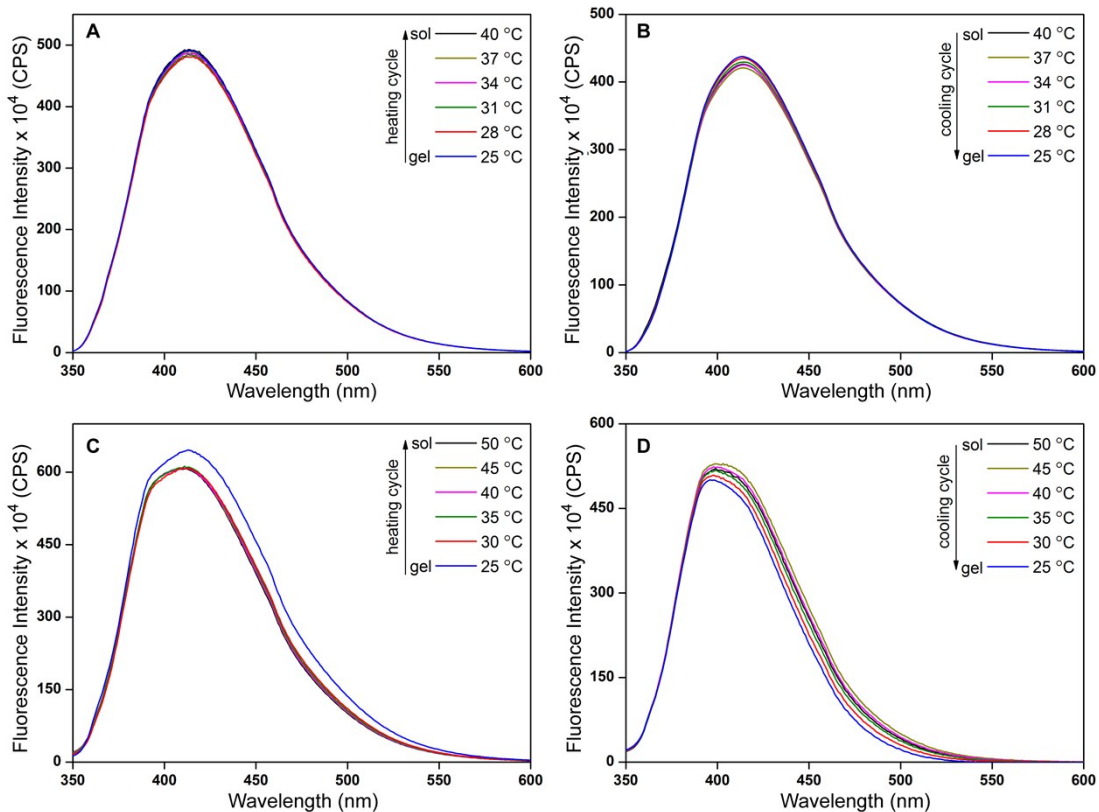


**Fig. S15** Fluorescence spectra of benzofuran-modified nucleolipid gels **5** and **6** at respective CGC as a function of temperature. Fluorescence spectra of **5** during heating (**A**) and cooling (**B**) cycles. Fluorescence spectra of **6** during heating (**C**) and cooling (**D**) cycles. Gels of **5** and **6** retained their fluorescence intensity in gel and solution states during heating and cooling cycles. Samples were excited at 320 nm with excitation and emission slit widths of 2 nm.

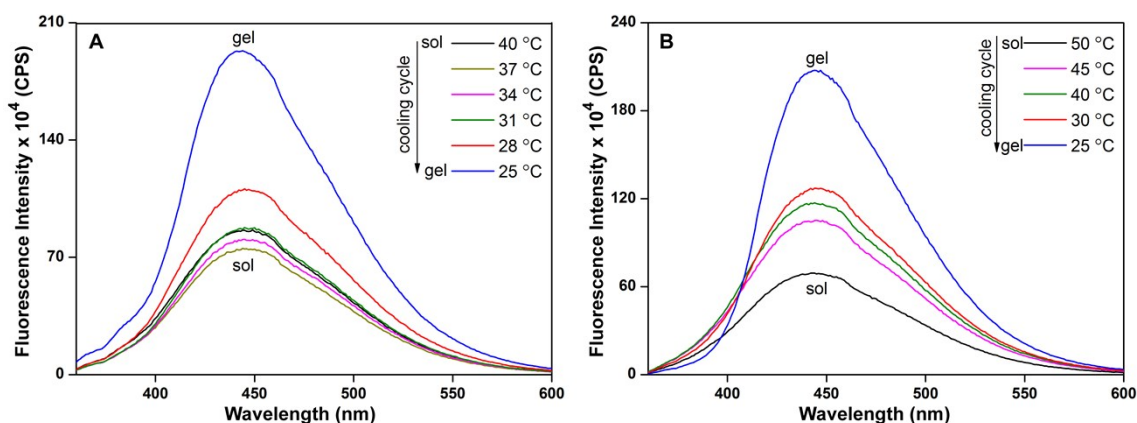


**Fig. S16** Fluorescence spectra of benzothiophene-modified nucleolipid gel **9** and **10** at respective CGC as a function of temperature. Fluorescence spectra of **9** (**A**) and **10** (**B**) during cooling cycle. As the nucleolipid solutions were gradually cooled to form the gels, a significant increase in fluorescence intensity was observed. Samples were excited at 320 nm with excitation and emission slit widths of 2 nm.

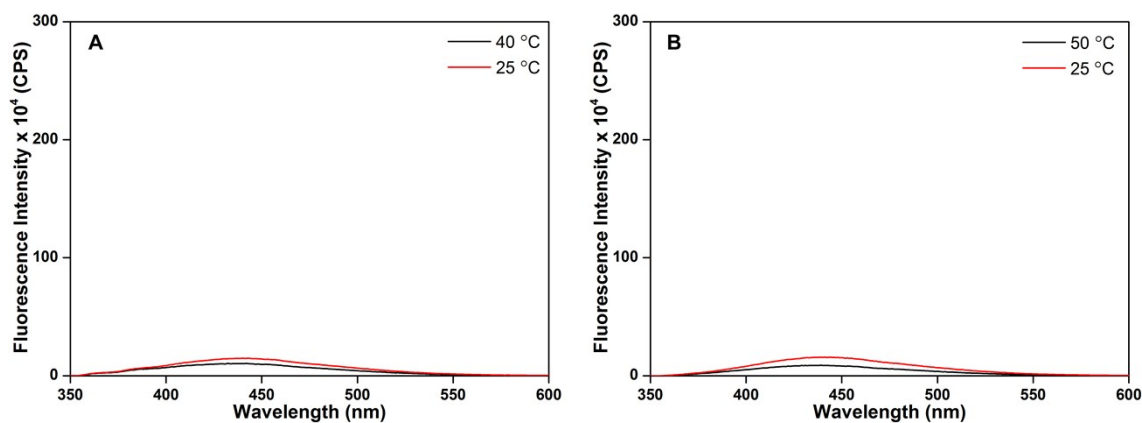


**Fig. S17** Fluorescence spectra of nucleolipid **9** (A) and **10** (B) at different temperatures. The fluorescence of nucleolipids (5  $\mu\text{M}$ ) at well below the CGC was not affected by changes in temperature. Samples were excited at 320 nm with excitation and emission slit widths of 2 nm. The Y-axis scale has been kept similar to that of Fig. 8 for better comparison.

## 7. Responsiveness of nucleolipid gel **10** to chemical stimuli.

*Effect of anions.* To a hot solution of nucleolipid **10** (1.4 w/v %) in DMSO was added increasing concentration of tetrabutylammonium salts of  $\text{F}^-$ ,  $\text{AcO}^-$ ,  $\text{Cl}^-$ ,  $\text{Br}^-$ ,  $\text{I}^-$  and  $\text{HSO}_4^-$  without altering the CGC of the gelator. The samples were allowed to stand at RT temperature for 1 h and the gelling ability was tested by inverted vial method. In the presence of  $\text{F}^-$  and  $\text{AcO}^-$  (0.5 equiv), nucleolipid **10** did not show any signs of gelation even after a month. The gelation was restored by addition of acetic acid (0.5 equiv). However,  $\text{Cl}^-$ ,  $\text{Br}^-$ ,  $\text{I}^-$  and  $\text{HSO}_4^-$  (5 equiv) did not affect the gelation process and formed stable gels within 20 min, which did not disintegrate for months at RT. The fluorescence of gel samples in the presence and absence of anions was recorded by exciting the samples at 320 nm with an excitation slit width of 2 nm and an emission slit width of 2 nm.

*Effect of base.* To a hot solution of nucleolipid **10** (1.4 w/v %) in DMSO was added increasing concentration a strong organic base, 1,8-diazabicyclo(5.4.0) undec-7-ene (DBU). The sample was allowed to stand at RT temperature for 1 h. The gelation test and fluorescence was recorded as above. DBU (0.5 equiv) arrested the gelation process, and subsequent addition of trichloroacetic acid (0.5 equiv) restored the gelling ability of **10**.

*Effect of metal ions.* To a hot solution of nucleolipid **10** (1.4 w/v %) in DMSO was added increasing concentration of  $\text{Hg}(\text{ClO}_4)_2 \cdot 6\text{H}_2\text{O}$ ,  $\text{Hg}(\text{NO}_3)_2 \cdot \text{H}_2\text{O}$ ,  $\text{Cd}(\text{OAc})_2 \cdot 2\text{H}_2\text{O}$ ,  $\text{Zn}(\text{NO}_3)_2 \cdot 6\text{H}_2\text{O}$ ,  $\text{AgNO}_3$  and  $\text{Pb}(\text{NO}_3)_2$  without altering the CGC of gelator. The samples were allowed to stand at RT temperature for 1 h and the fluorescence was recorded as above. While  $\text{Hg}^{2+}$  lead to the precipitation, other metal ions tested did not affect the gelling ability of **10**.

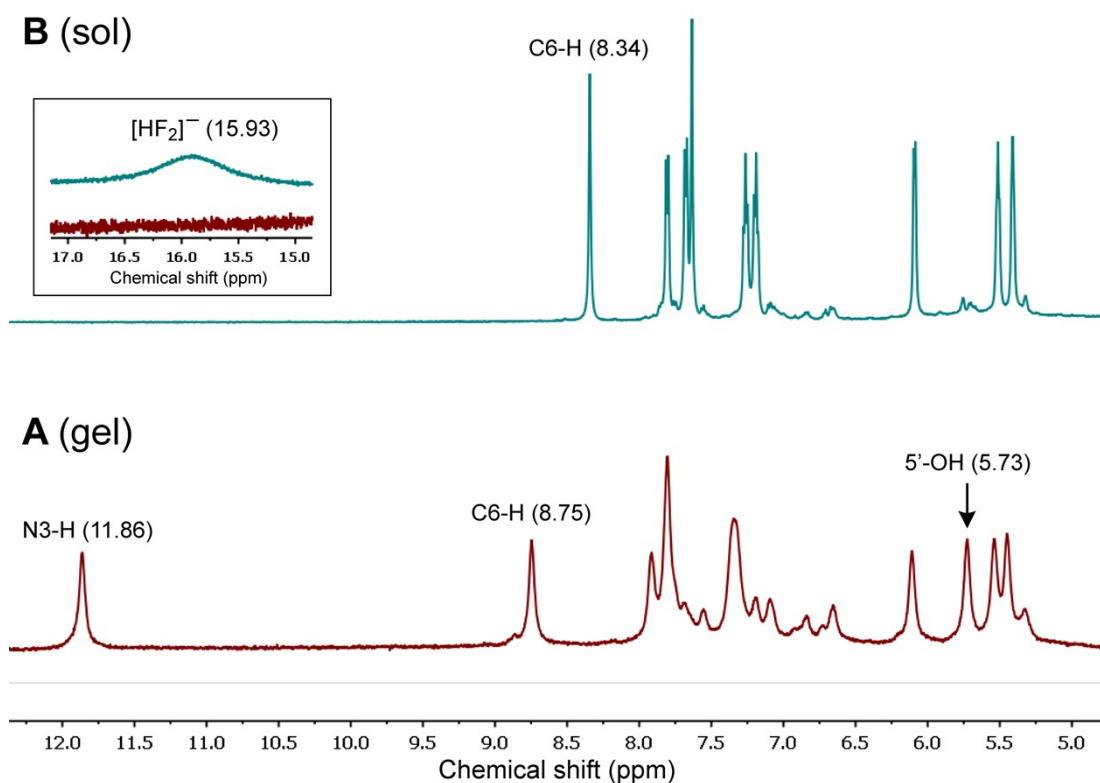


**Fig. S18** Partial  $^1\text{H}$  NMR spectrum of nucleolipid **10** in  $d_6$ -DMSO (1.4 w/v%) in the absence (**A**, gel state) and presence of 3 equivalence of fluoride ion (**B**, sol state). The disappearance of N3H (11.86 ppm) and 5'-OH (5.73 ppm) signals and appearance of a new broad signal at 15.93 ppm corresponding to  $\text{HF}_2^-$  confirms the deprotonation of imino and 5'-O hydrogen atoms by fluoride anion.  $^1\text{H}$  NMR spectra were obtained using Bruker 500 MHz spectrometer.

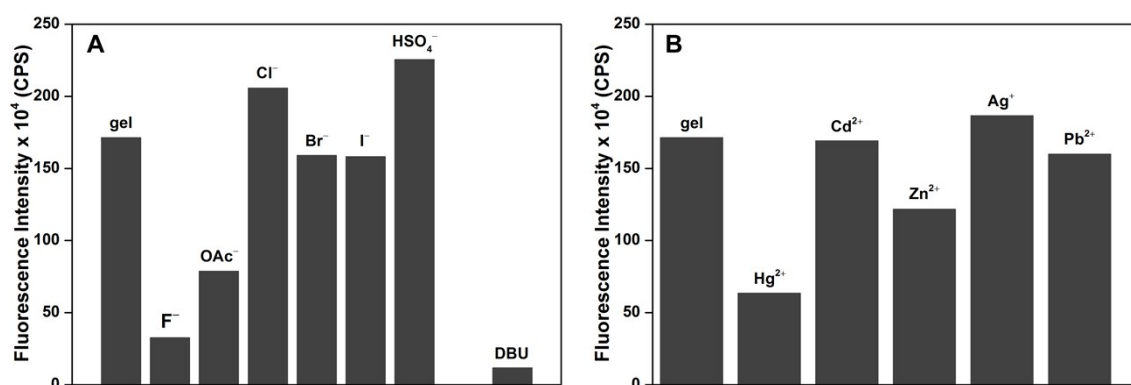


**Fig. S19** Plots showing the effect of addition of anions, a base and metal ions on the fluorescence intensity ( $\lambda_{\text{em}} = 445$  nm) of benzothiophene-modified nucleolipid gel **10**. Fluorescence spectra were recorded by exciting the samples at 320 nm with excitation and emission slit widths of 2 nm. **(A)** Fluorescence intensity of **10** in the presence of various anions. Addition of  $\text{F}^-$  and  $\text{AcO}^-$  completely arrested the gel formation and displayed significant reduction in fluorescence intensity in sol state. Other anions tested did not affect the gelation of **10**. Addition of a strong organic base, 1,8-diazabicyclo(5.4.0) undec-7-ene (DBU), arrested the gelation process and resulted in significant reduction in fluorescence intensity in sol state. **(B)** Fluorescence intensity of **10** in the presence of various metal ions. Among the metal ions tested addition of  $\text{Hg}^{2+}$  alone lead to the precipitation of **10** and reduction ( $\sim 3$ -fold) in fluorescence intensity.

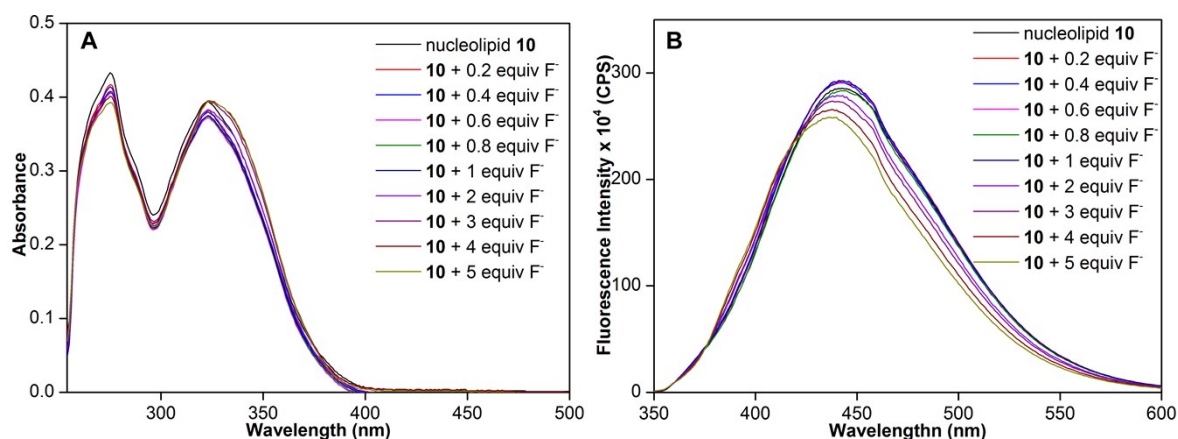


**Fig. S20** Effect of fluoride ion on UV absorption (**A**) and fluorescence (**B**) of nucleolipid **10** at well below its CGC. Concentration of **10** for absorption and fluorescence analysis was 25  $\mu\text{M}$  and 10  $\mu\text{M}$ , respectively. Samples were excited at 320 nm with an excitation slit width of 2 nm and emission slit width of 2 nm. Only small changes in absorption and fluorescence profile upon addition of fluoride ion were observed.

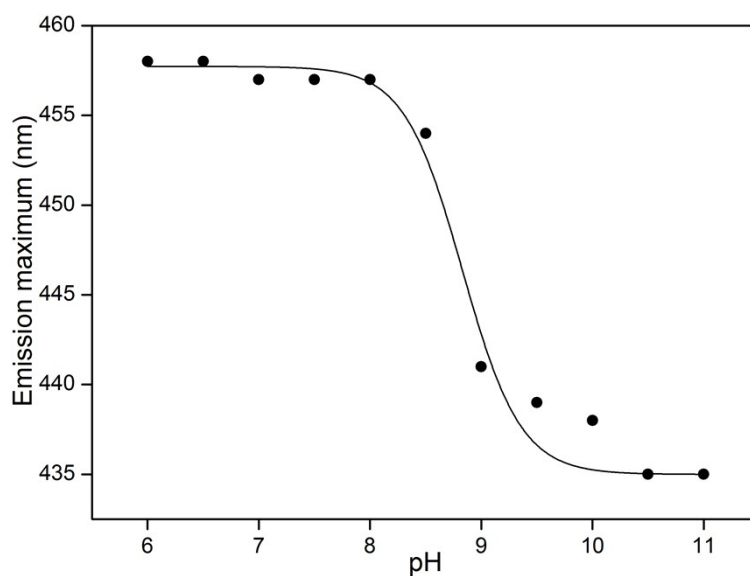


**Fig. S21** A plot of emission maximum of benzothiophene-modified uridine nucleoside versus pH. The  $pK_a$  of N3-H of benzothiophene-modified uridine nucleoside (10  $\mu\text{M}$ ) in aqueous buffer was determined by fitting the changes in emission maximum as a function of pH. The curve fit gave a  $pK_a$  of  $9.0 \pm 0.1$ . Under these condition there was no significant changes in fluorescence intensity.

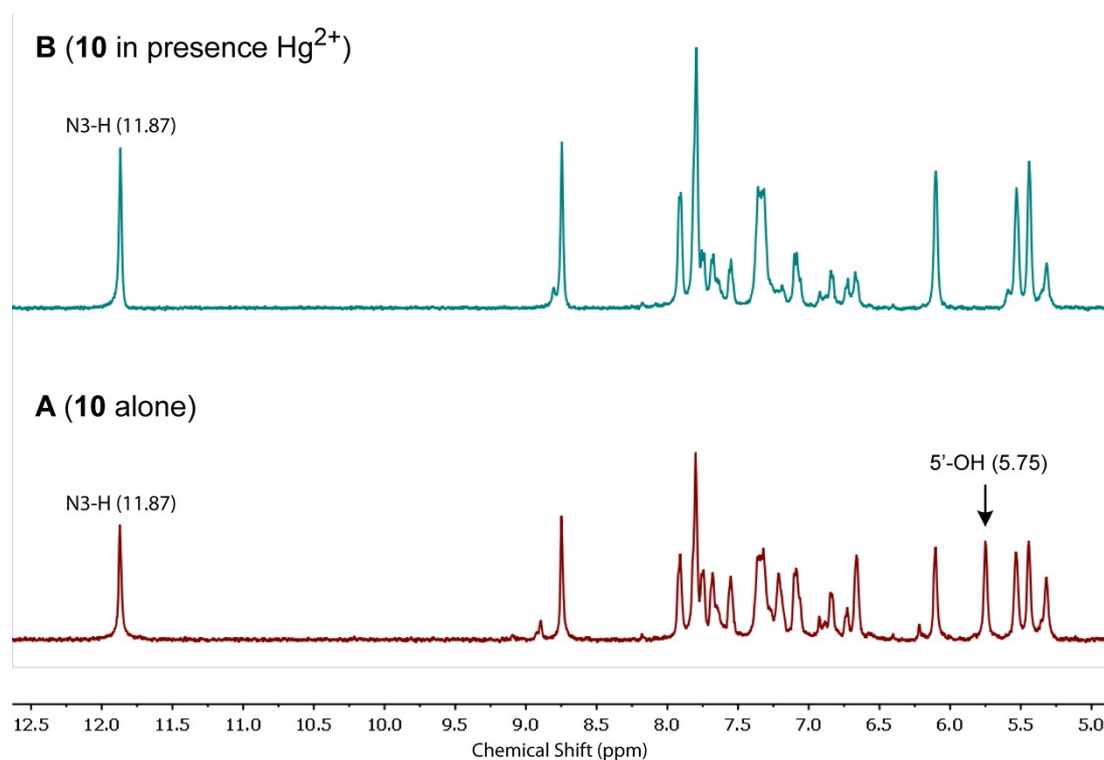


**Fig. S22** Partial  $^1\text{H}$  NMR spectrum of nucleolipid gel **10** in  $d_6$ -DMSO (1.4 w/v %) in the absence (**A**) and presence of 1 equivalence of  $\text{Hg}^{2+}$  ion (**B**). Addition of  $\text{Hg}^{2+}$  ion did not affect N3-H signal (11.87 ppm), but resulted in the disappearance of 5'-OH signal (5.75 ppm). The deprotonation of 5'-OH due to binding of mercury to nucleolipid is the likely reason for the disruption of H-bonding interaction, and hence, the gelling ability of the nucleolipid.<sup>S5,S6</sup>

**Table S2. Crystallographic data for nucleolipid 5**

Compound identity	<b>5</b>
CCDC (deposition number)	1423164
Empirical formula	$\text{C}_{45}\text{H}_{68}\text{N}_2\text{O}_9$
Formula weight	781.04
Temperature	100(2) K
Wavelength	0.71073 Å
Crystal system	Triclinic
Space group	P 1
Unit cell dimensions	a = 8.615(3) Å $\alpha$ = 101.343(7) b = 11.124(4) Å $\beta$ = 91.424(7) c = 25.315(9) Å $\gamma$ = 109.601(6)
Volume	2229.9(14) Å <sup>3</sup>
Z	2
Density (calculated)	1.218 Mg/cm <sup>3</sup>
Absorption coefficient ( $\mu$ )	0.084 mm <sup>-1</sup>
F(000)	888
Crystal size	0.40 X 0.17 X 0.05 mm <sup>3</sup>
Theta range for data collection	4.11 to 28.28
Index ranges	-11 ≤ h ≤ 11, -14 ≤ k ≤ 10, -31 ≤ l ≤ 33
Reflections collected	32572
Independent reflections	13635 [R(int) = 0.0985]
Completeness to theta = 28.28	97.0 %
Absorption correction	MULTI-SCAN

Max. and min. Transmission	0.983 and 0.996
Refinement method	Full-matrix least-squares on F <sup>2</sup>
Data / restraints / parameters	13635 / 9 / 1063
Goodness-of-fit on F <sup>2</sup>	0.958
Final R indices [I>2sigma(I)]	R1 = 0.0652, wR2 = 0.1124
R indices (all data)	R1 = 0.1361, wR2 = 0.1372
Largest diff. Peak and hole	0.285 and -0.288 e.Å <sup>-3</sup>

**Table S3. Crystallographic data for nucleolipid 6**

Compound identity	<b>6</b>
CCDC (deposition number)	1423177
Empirical formula	C <sub>49</sub> H <sub>76</sub> N <sub>2</sub> O <sub>9</sub>
Formula weight	836.55
Temperature	100(2) K
Wavelength	0.71073 Å
Crystal system	Triclinic
Space group	P1
Unit cell dimensions	a = 8.671(7) α = 94.389(14) b = 11.183(9) β = 97.977(16) c = 27.36(2) γ = 109.553(14)
Volume	2455(4) Å <sup>3</sup>
Z	2
Density (calculated)	1.182 Mg/cm <sup>3</sup>
Absorption coefficient (μ)	0.081 mm <sup>-1</sup>
F(000)	952
Crystal size	0.39 X 0.19 X 0.05 mm <sup>3</sup>
Theta range for data collection	4.10 to 25.02
Index ranges	-10<=h<=9, -13<=k<=13, -32<=l<=32
Reflections collected	32275
Independent reflections	11984[R(int) = 0.3614]
Completeness to theta = 25.02	99.4 %
Absorption correction	MULTI-SCAN
Max. and min. Transmission	0.982 and 0.996
Refinement method	Full-matrix least-squares on F <sup>2</sup>
Data / restraints / parameters	11984 / 45 / 1134
Goodness-of-fit on F <sup>2</sup>	0.643
Final R indices [I>2sigma(I)]	R1 = 0.0725, wR2 = 0.1467
R indices (all data)	R1 = 0.2949, wR2 = 0.2409
Largest diff. Peak and hole	0.239 and -0.262 e.Å <sup>-3</sup>

**Table S4. Crystallographic data for nucleolipid 9**

Compound identity	<b>9</b>
CCDC (deposition number)	1423141
Empirical formula	C <sub>45</sub> H <sub>68</sub> N <sub>2</sub> O <sub>8</sub> S
Formula weight	796.46
Temperature	296(2) K
Wavelength	0.71073 Å
Crystal system	Triclinic
Space group	P1
Unit cell dimensions	a = 5.4174(5) α = 95.858(2) b = 9.3296(9) β = 92.994(2) c = 24.033(2) γ = 93.330(2)

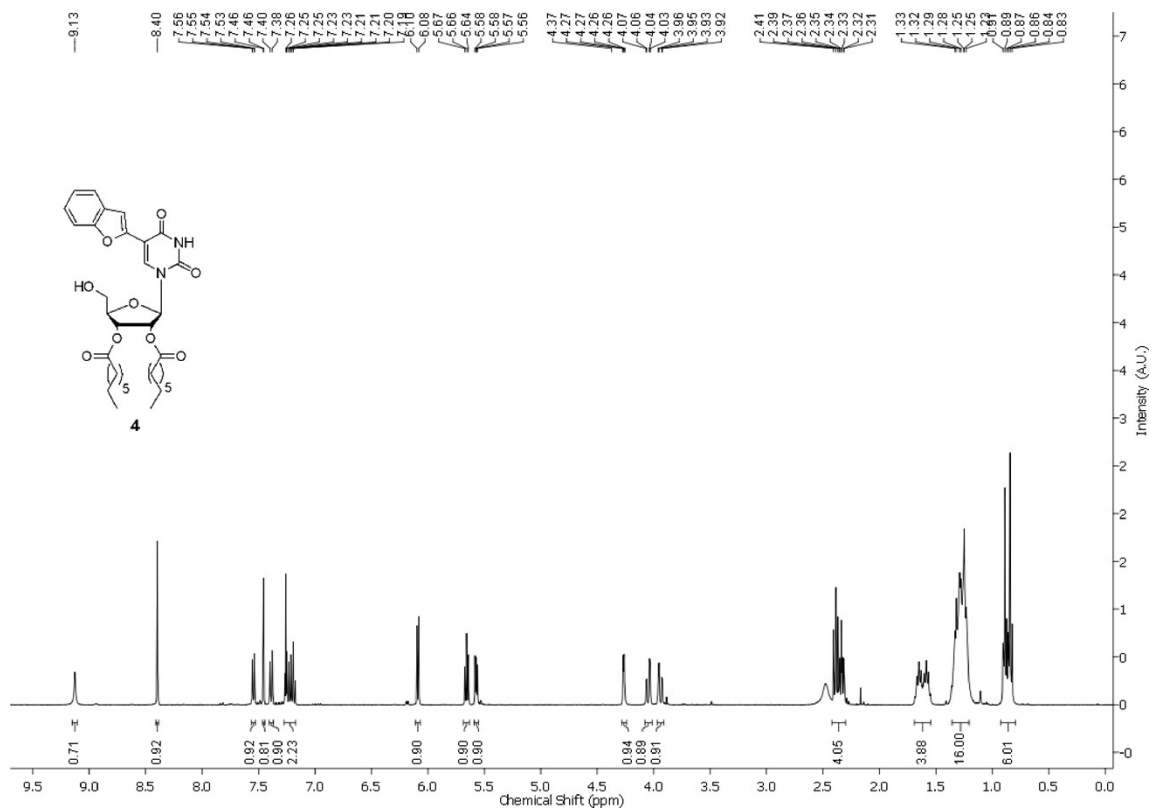
Volume	1204.2(2)
Z	2
Density (calculated)	1.207 Mg/cm <sup>3</sup>
Absorption coefficient ( $\mu$ )	0.122 mm <sup>-1</sup>
F(000)	474
Crystal size	0.35 X 0.15 X 0.04 mm <sup>3</sup>
Theta range for data collection	4.23 to 27.59
Index ranges	-7<=h<=7, -12<=k<=9, -30<=l<=31
Reflections collected	40246
Independent reflections	8197[R(int) = 0.0612]
Completeness to theta = 27.59	99.2 %
Absorption correction	MULTI-SCAN
Max. and min. Transmission	0.978 and 0.995
Refinement method	Full-matrix least-squares on F <sup>2</sup>
Data / restraints / parameters	8197 / 9 / 520
Goodness-of-fit on F <sup>2</sup>	1.054
Final R indices [I>2sigma(I)]	R1 = 0.0676, wR2 = 0.1557
R indices (all data)	R1 = 0.0918, wR2 = 0.1700
Largest diff. Peak and hole	0.723 and -0.661 e.Å <sup>-3</sup>

**Table S5. Crystallographic data for nucleolipid 10**

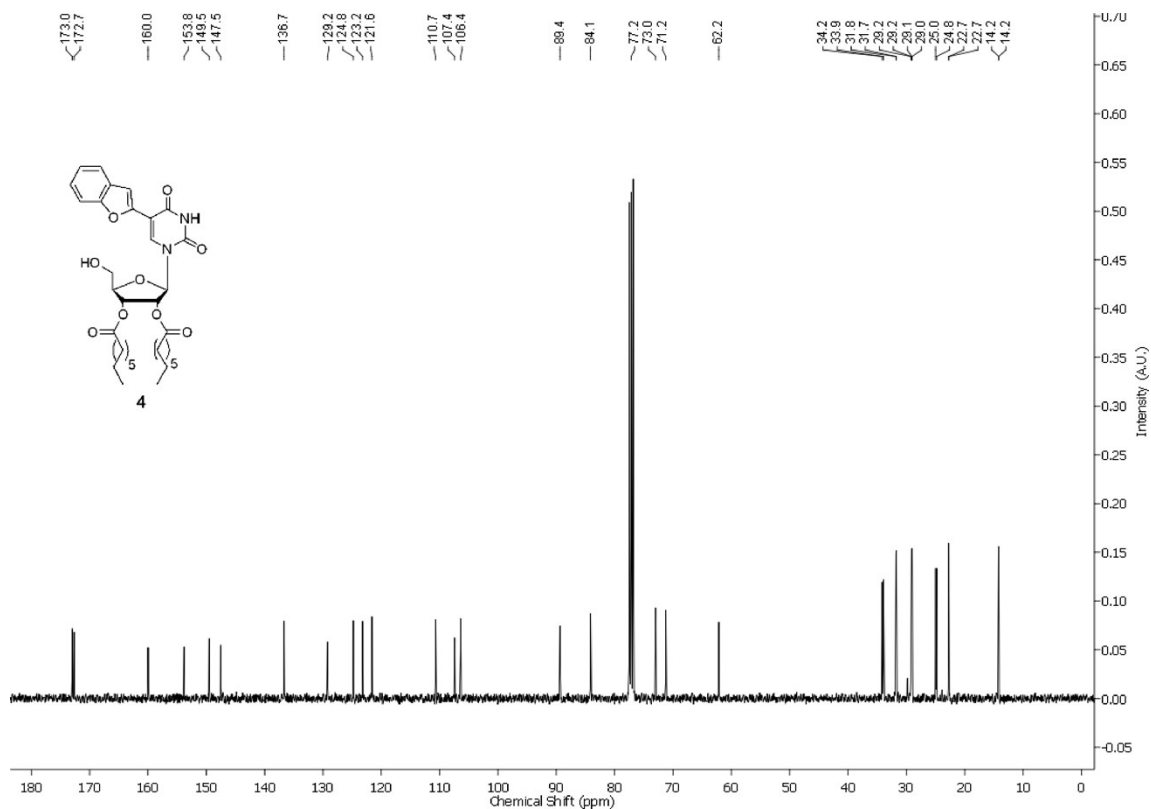
Compound identity	<b>10</b>
CCDC (deposition number)	1423142
Empirical formula	C <sub>49</sub> H <sub>76</sub> N <sub>2</sub> O <sub>8</sub> S
Formula weight	852.53
Temperature	296(2) K
Wavelength	0.71073 Å
Crystal system	Triclinic
Space group	P1
Unit cell dimensions	a = 5.385(8) Å $\alpha$ = 92.65(2) b = 9.274(13) Å $\beta$ = 95.509(19) c = 25.69(4) Å $\gamma$ = 93.348(20)
Volume	1273(3)
Z	1
Density (calculated)	1.215 Mg/cm <sup>3</sup>
Absorption coefficient ( $\mu$ )	0.119 mm <sup>-1</sup>
F(000)	506
Crystal size	0.39 X 0.18 X 0.03 mm <sup>3</sup>
Theta range for data collection	4.27 to 25.02
Index ranges	-6<=h<=6, -10<=k<=10, -30<=l<=30
Reflections collected	11701
Independent reflections	5427[R(int) = 0.1855]
Completeness to theta = 25.02	92.2 %
Absorption correction	MULTI-SCAN
Max. and min. Transmission	0.975 and 0.996
Refinement method	Full-matrix least-squares on F <sup>2</sup>
Data / restraints / parameters	5427 / 168 / 569
Goodness-of-fit on F <sup>2</sup>	1.001
Final R indices [I>2sigma(I)]	R1 = 0.1082, wR2 = 0.2511
R indices (all data)	R1 = 0.2437, wR2 = 0.3229
Largest diff. Peak and hole	0.449 and -0.428 e.Å <sup>-3</sup>

## 8. NMR spectra

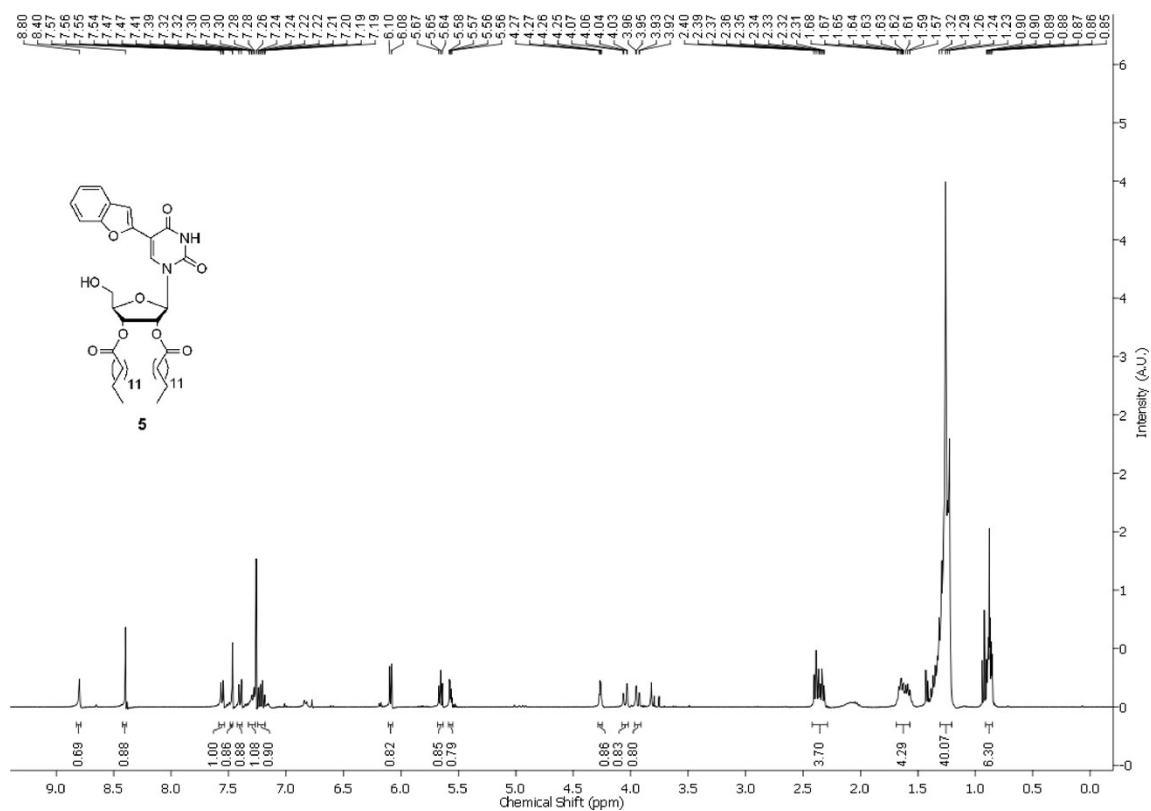
### $^1\text{H}$ NMR of nucleolipid **4** in $\text{CDCl}_3$



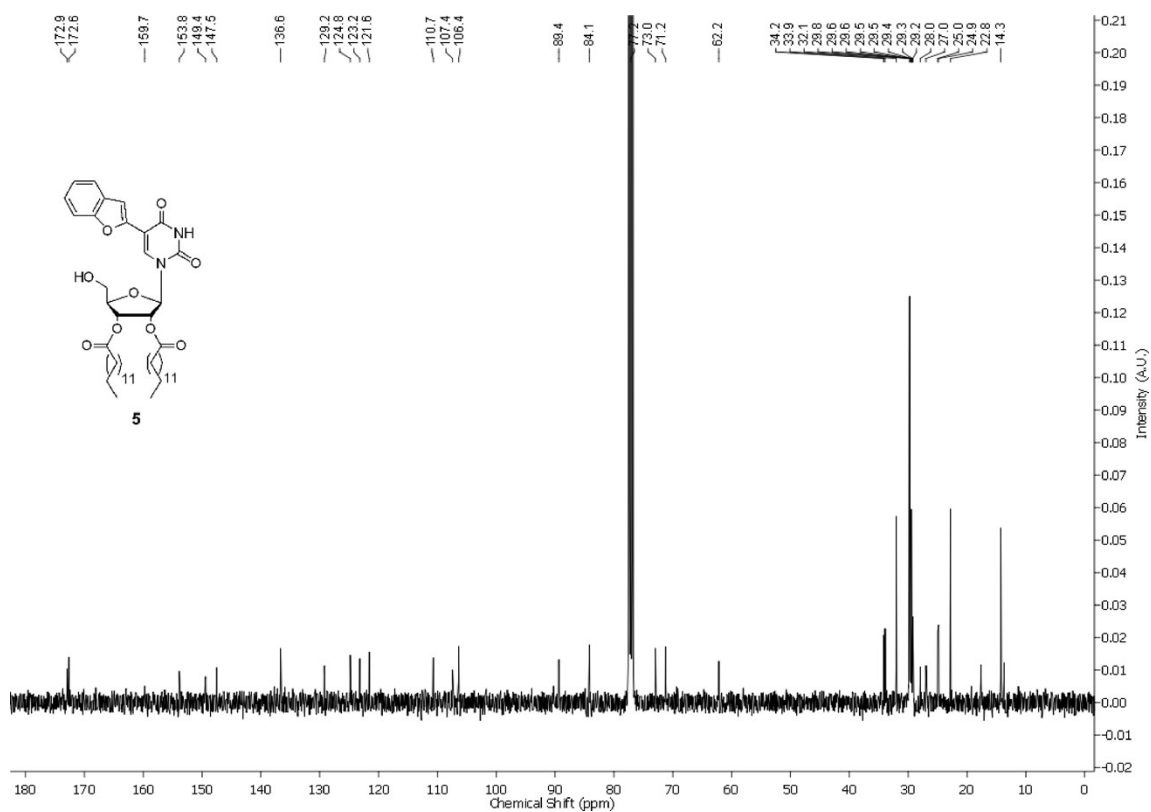
### $^{13}\text{C}$ NMR of nucleolipid **4** in $\text{CDCl}_3$



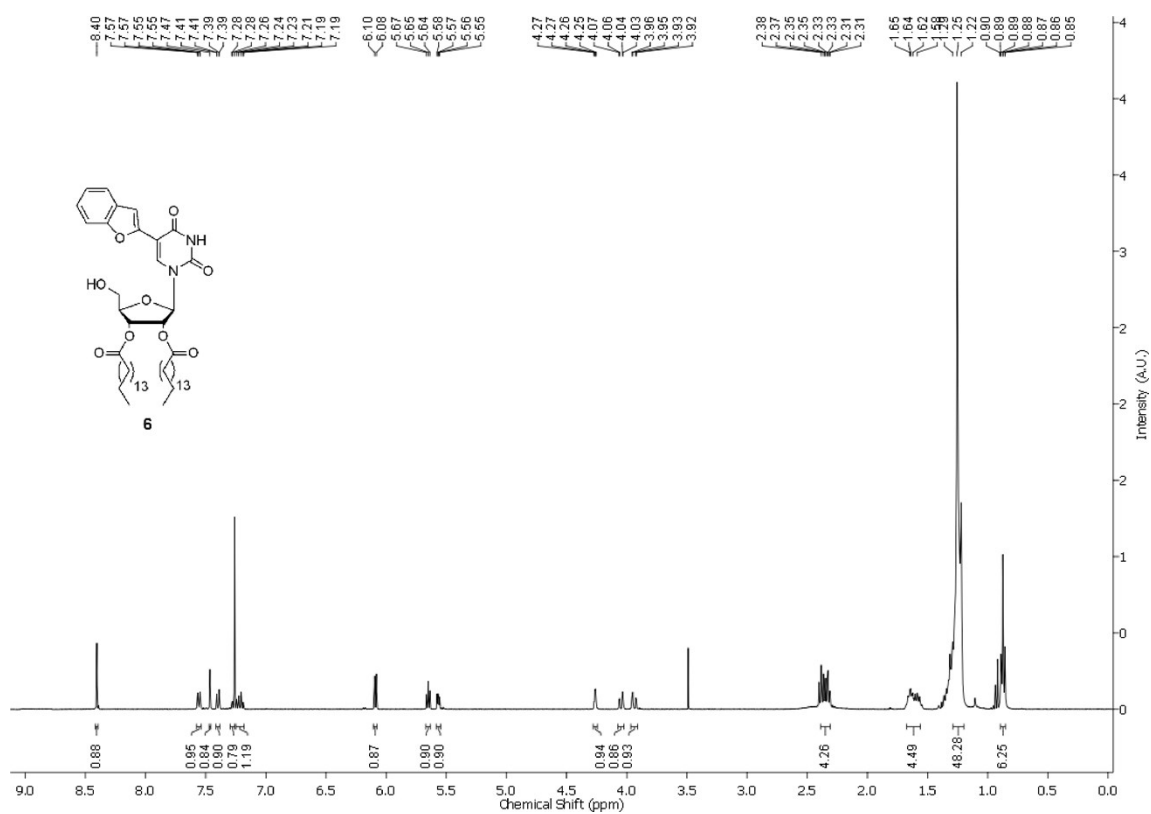
<sup>1</sup>H NMR of nucleolipid **5** in CDCl<sub>3</sub>



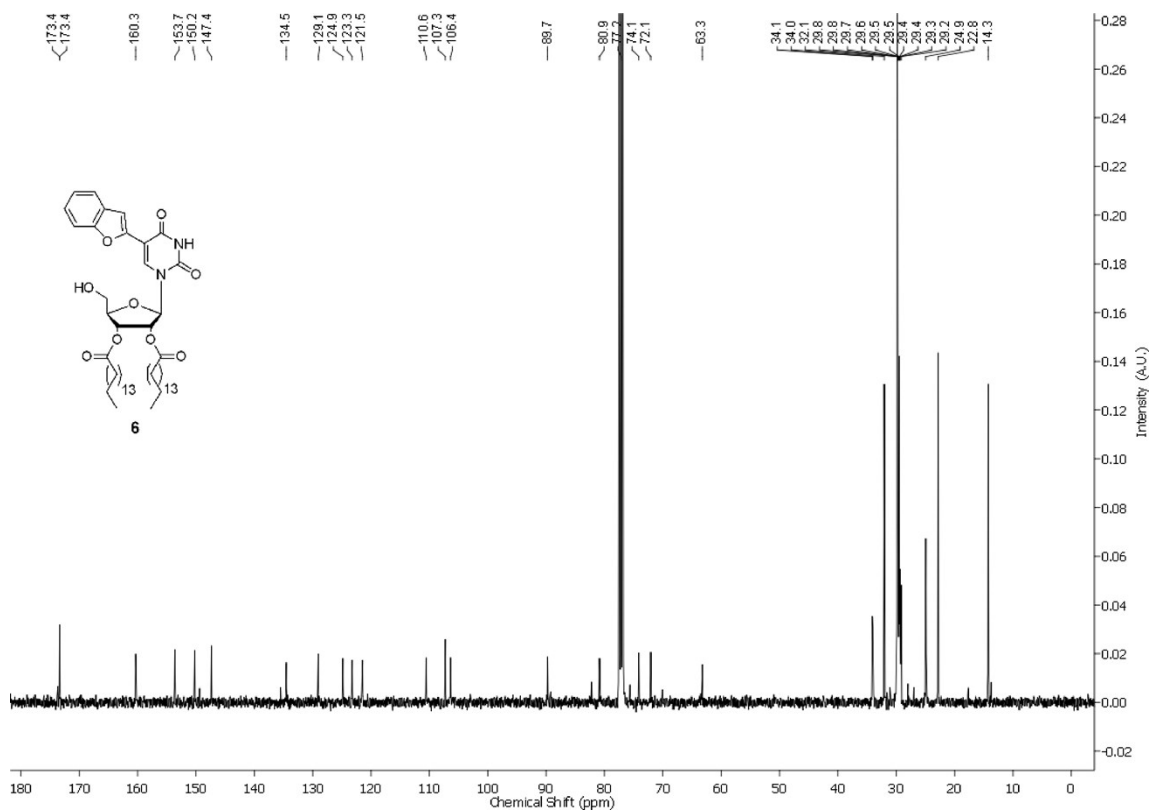
<sup>13</sup>C NMR of nucleolipid **5** in CDCl<sub>3</sub>



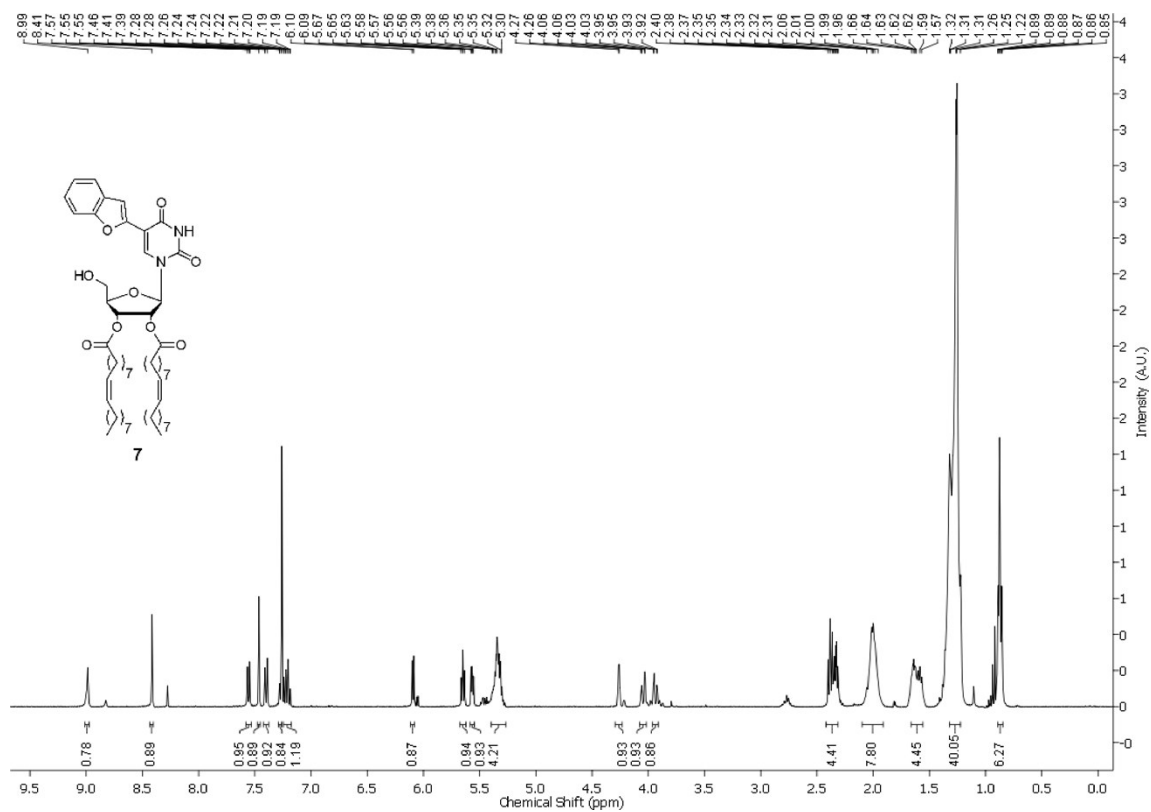
### $^1\text{H}$ NMR of nucleolipid **6** in $\text{CDCl}_3$



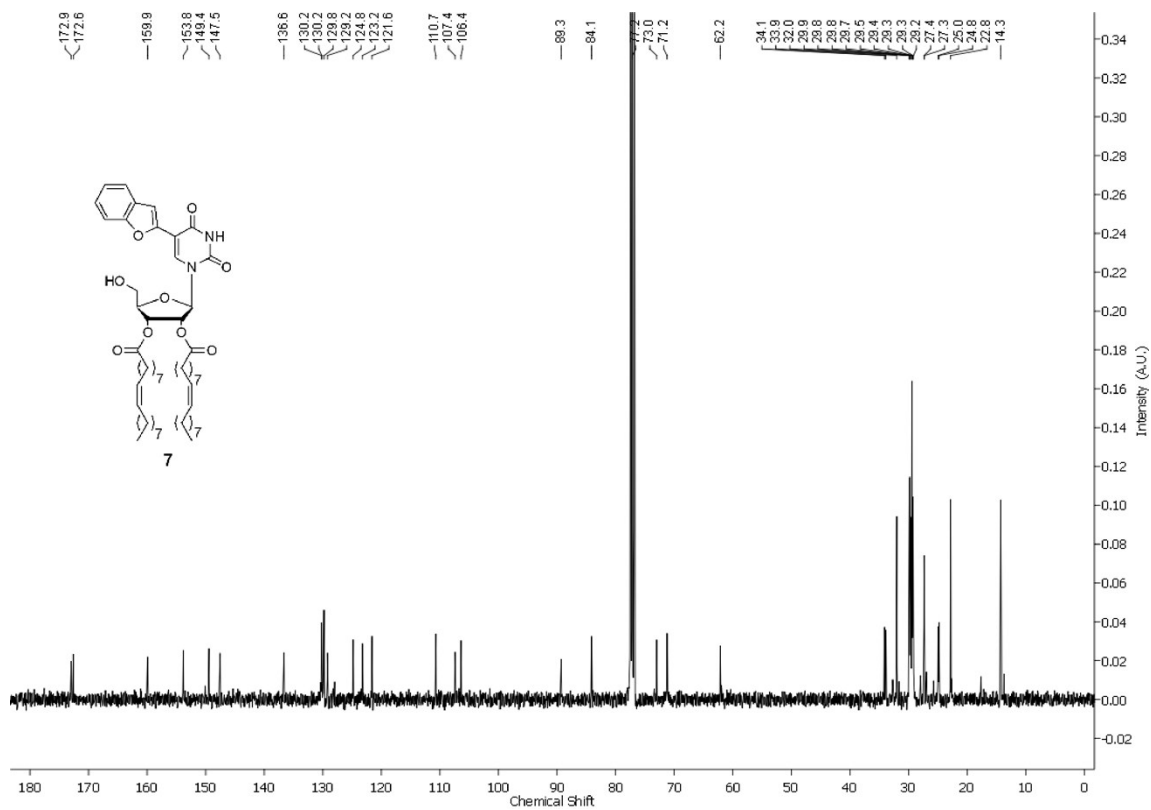
### $^{13}\text{C}$ NMR of nucleolipid **6** in $\text{CDCl}_3$



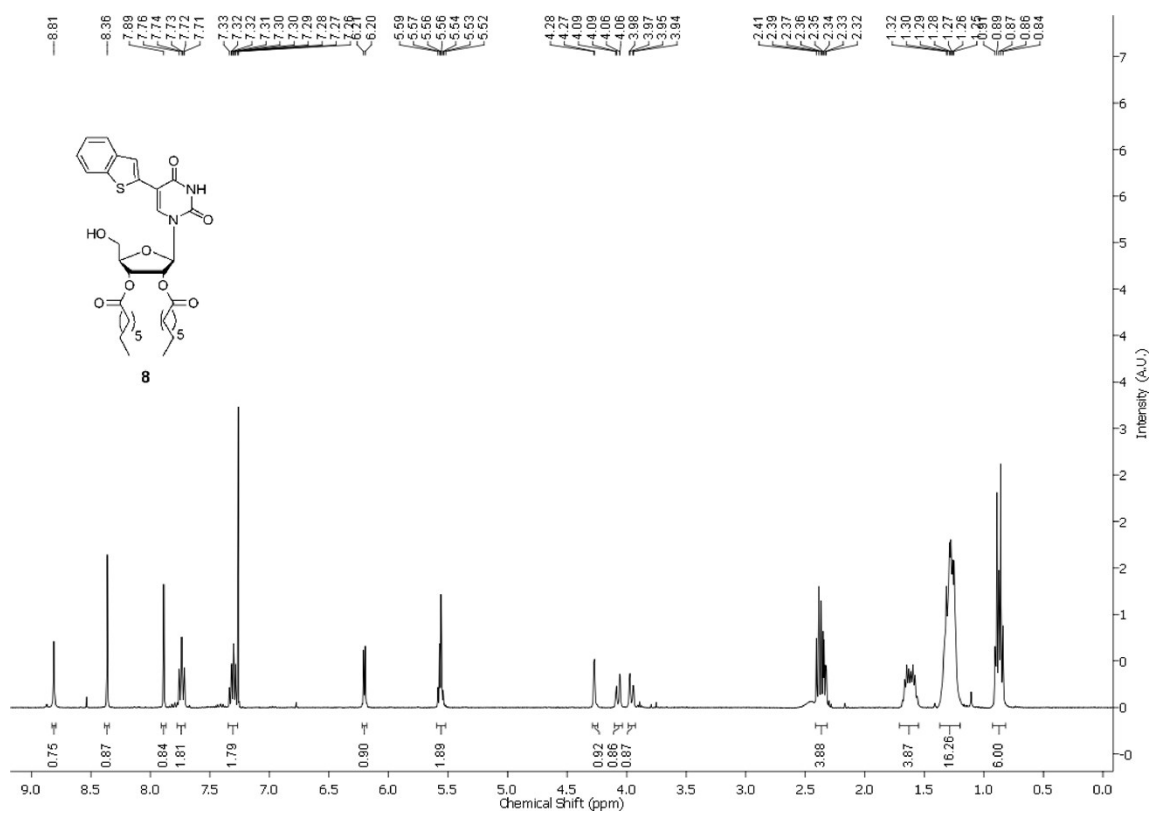
### <sup>1</sup>H NMR of nucleolipid **7** in CDCl<sub>3</sub>



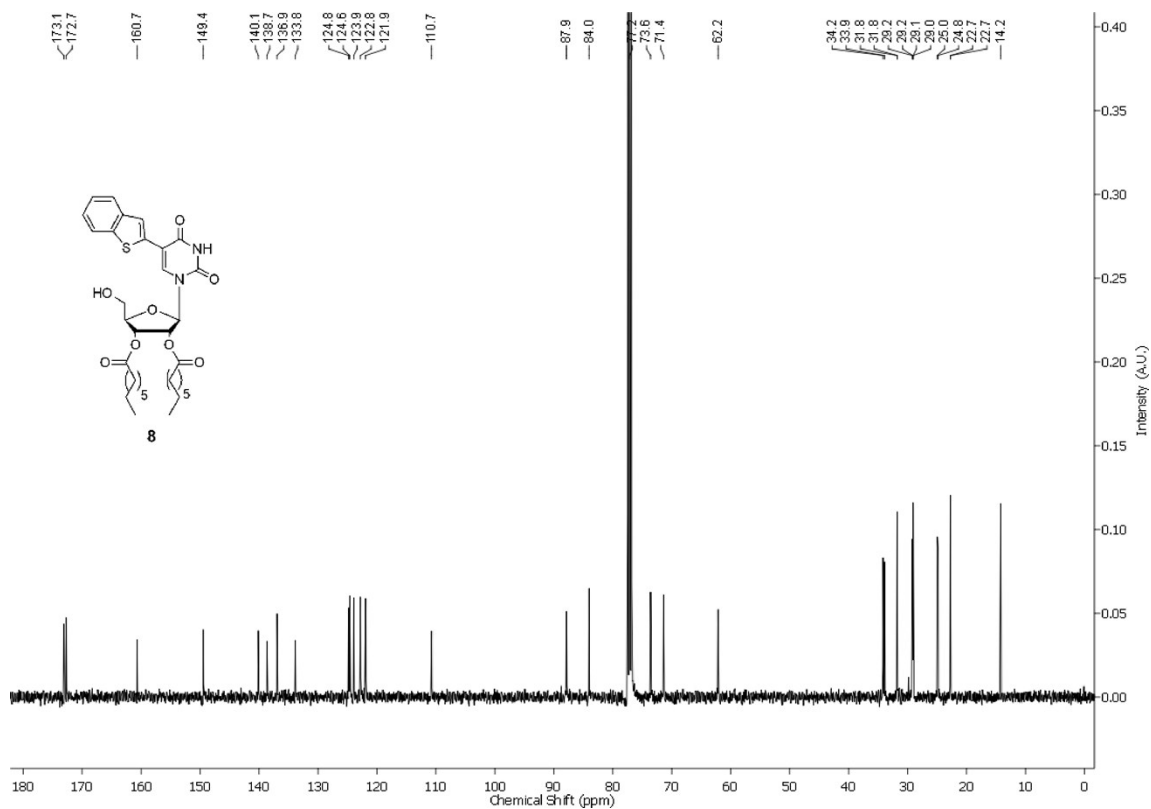
### <sup>13</sup>C NMR of nucleolipid **7** in CDCl<sub>3</sub>



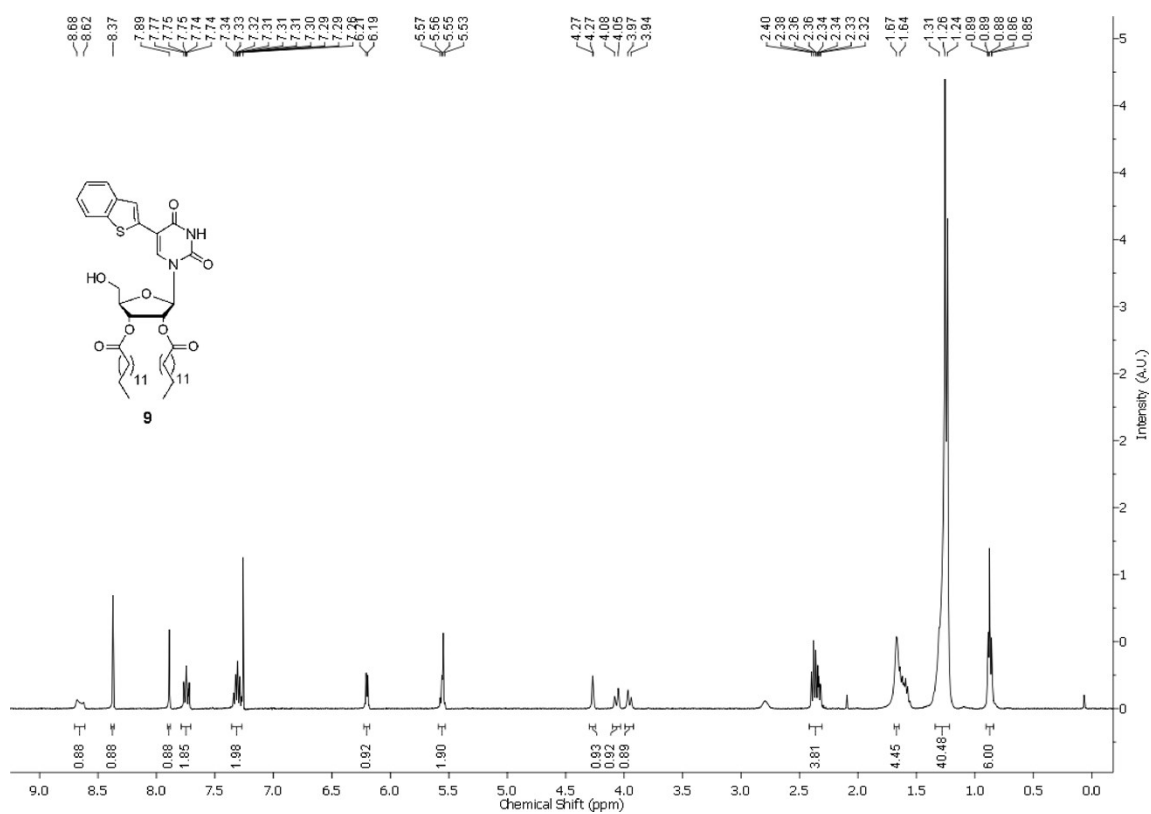
# $^1\text{H}$ NMR of nucleolipid **8** in $\text{CDCl}_3$



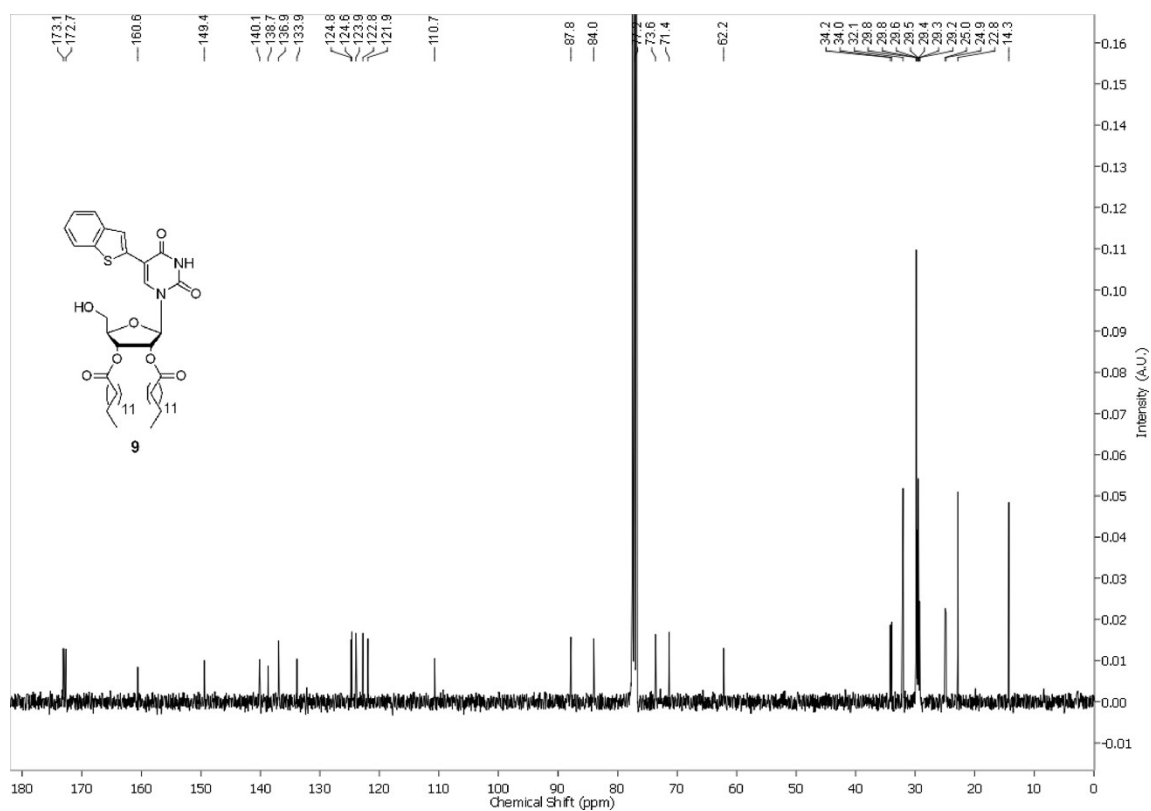
# $^{13}\text{C}$ NMR of nucleolipid **8** in $\text{CDCl}_3$



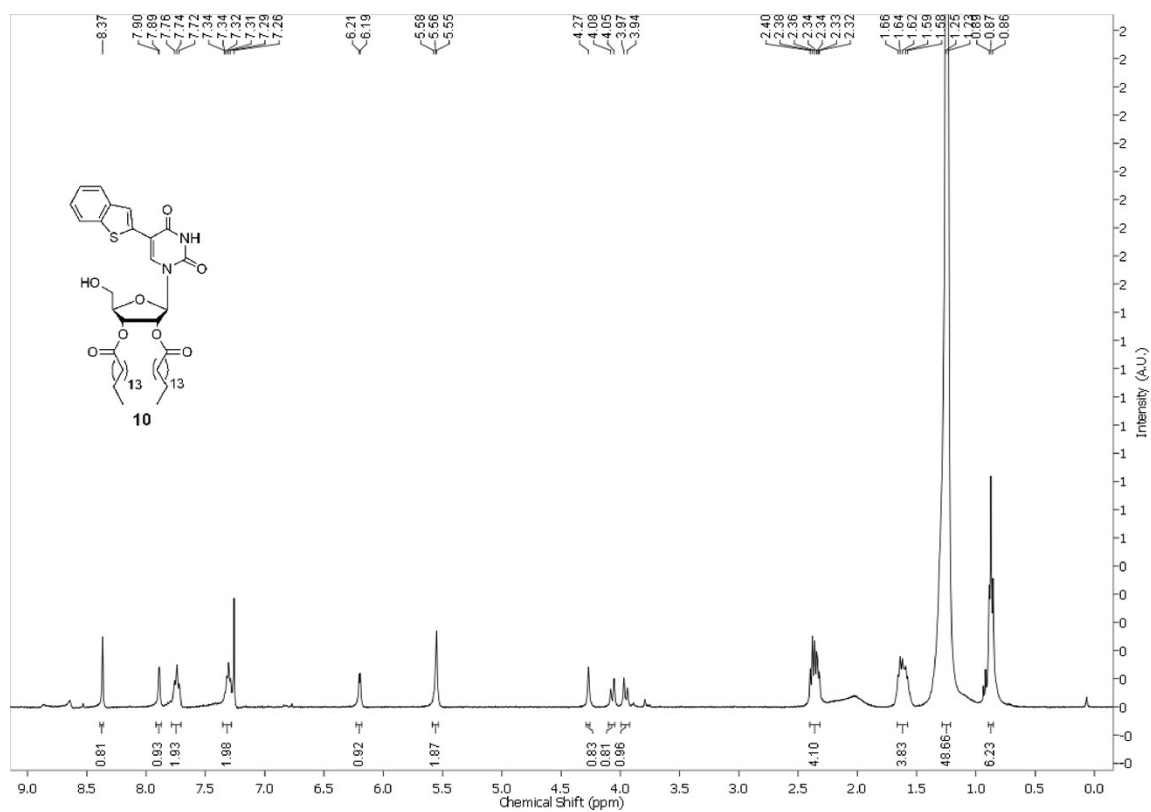
### $^1\text{H}$ NMR of nucleolipid **9** in $\text{CDCl}_3$



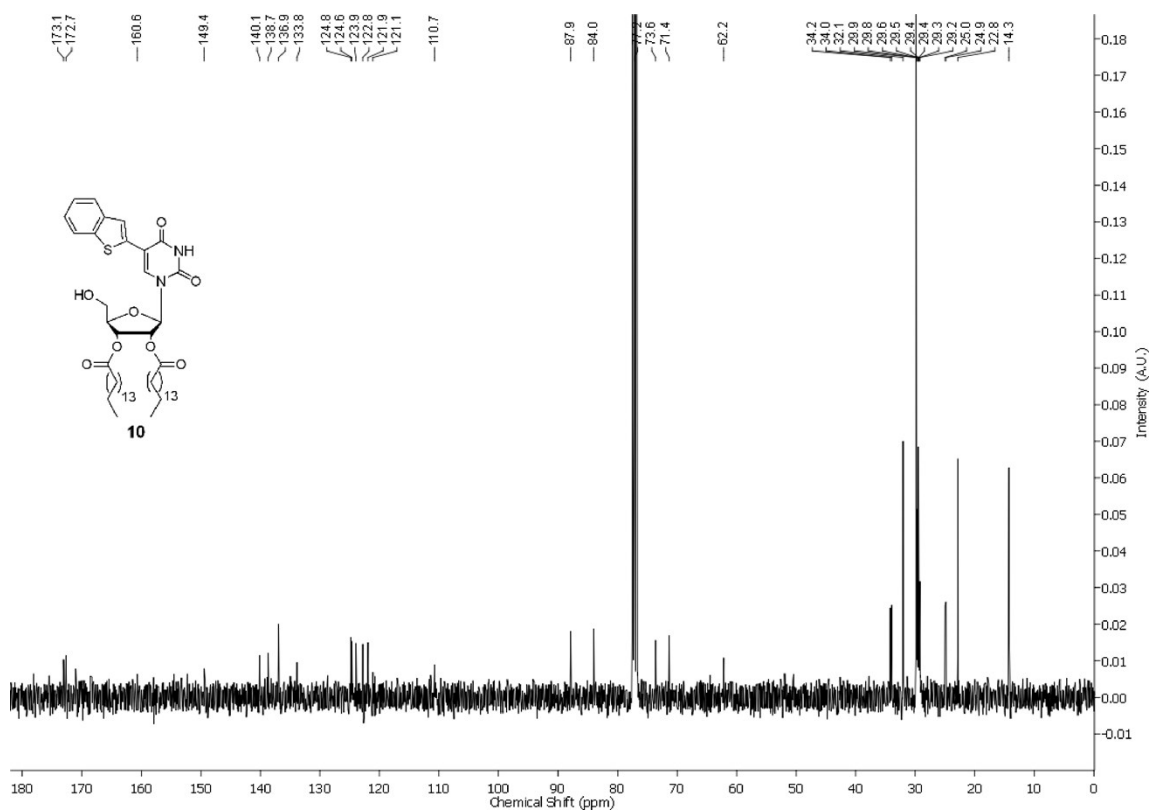
### $^{13}\text{C}$ NMR of nucleolipid **9** in $\text{CDCl}_3$



### $^1\text{H}$ NMR of nucleolipid **10** in $\text{CDCl}_3$



### $^{13}\text{C}$ NMR of nucleolipid **10** in $\text{CDCl}_3$





## 9. References

- S1. K. Shah, H. Wu and T. M. Rana, *Bioconjugate Chem.*, 1994, **5**, 508–512.
- S2. L. S. Liebeskind and J. Wang, *J. Org. Chem.*, 1993, **58**, 3550–3556.
- S3. D. Lavabre and S. Fery-Forgues, *J. Chem. Educ.*, 1999, **76**, 1260–1264.
- S4. D. C. Ward, E. Reich and L. Stryer, *J. Biol. Chem.*, 1969, **244**, 1228–1237.
- S5. E. M. Nolan and S. J. Lippard, *Chem. Rev.*, 2008, **108**, 3443–3480.
- S6. N. Kaur, G. Dhaka and J. Singh. *New J. Chem.*, 2015, **39**, 6125–6129.